8 Radio Telescopes

Ron Ekers[1] · *Thomas L. Wilson*[2]
[1]Australia Telescope National Facility, CSIRO Astronomy and Space Science, Epping, NSW, Australia
[2]Naval Research Laboratory, Washington, DC, USA

T.D. Oswalt, I.S. McLean (eds.), *Planets, Stars and Stellar Systems. Volume 1: Telescopes and Instrumentation*,
DOI 10.1007/978-94-007-5621-2_8,

Abstract: "Radio Telescopes" starts with a brief historical introduction from Jansky's 1931 discovery of radio emission from the Milky Way through the development of radio telescope dishes and arrays to aperture synthesis imaging. It includes sufficient basics of electromagnetic radiation to provide some understanding of the design and operation of radio telescopes. The criteria such as frequency range, sensitivity, survey speed, angular resolution, and field of view that determine the design of radio telescopes are introduced**.** Because it is so easy to manipulate the electromagnetic waves at radio frequencies, radio telescopes have evolved into many different forms, sometimes with "wire" structures tuned to specific wavelengths, which look very different from any kind of classical telescope. To assist astronomers more familiar with other wavelength domains, the ❯ appendix A.1. includes a comparison of radio and optical terminology. Some of the different types of radio telescopes including the filled aperture dishes, electronically steered phased arrays, and aperture synthesis radio telescopes are discussed, and there is a section comparing the differences between dishes and arrays. Some of the more recent developments including hierarchical beam forming, phased array feeds, mosaicing, rotation measure synthesis, digital receivers, and long baseline interferometers are included. The problem of increasing radio frequency interference is discussed, and some possible mitigation strategies are outlined.

The open-sky policy adopted by most radio astronomy observatories makes it possible to select the best radio telescope for an experiment, and some guidelines are provided together with an ❯ appendix A.2. listing all of the world's large centimeter and meter radio wavelength telescopes. Finally, we include a short description of some of the great radio telescopes which have had the most scientific impact in the last decade and give some indications of future directions.

Keywords: Angular resolution, Aperture synthesis, Digital receivers, Field of view, History, Phased arrays, Radio telescopes, RFI, Sensitivity

1 Introduction

The intention is to give an overview of the history, design, and use of radio telescopes with emphasis on the general principals rather than detailed analysis. This should allow the astronomer to make informed decisions about the most suitable type of radio telescope to use to obtain observational information. Once this decision is made, most observatories will provide the tools needed to fine-tune sensitivity requirements and the other detailed specifications needed to make effective observations. These fundamentals are also essential when considering the design of future radio telescopes. The discussions of the basics is extended, and receivers, backends, and data processing are discussed in Volume 2, ❯ Chap. 6.

Volume 1, ❯ Chap. 7, covers submillimeter and millimeter radio telescopes, and we focus here on the wavelength range from about 30 GHz (1 cm) down to the ionospheric cutoff at about 15 MHz (20 m). This range of 2,000:1 in wavelength results in a great diversity in radio telescope designs.

Because it is so easy to manipulate the electromagnetic waves at radio frequencies, radio telescopes have evolved into many different forms, sometimes with "wire" structures tuned to specific wavelengths, which look very different from any kind of classical telescope. The most striking difference is between the dishes which are single monolithic collectors, either parabolic or parabolic sections, which concentrate the radiation at the focus where it is amplified in radio receivers, and the arrays which involve many separated receptors which sample the wave

front over large areas in the aperture plane and form an image by combining these signals electronically. In either case, the receiver amplifies the power collected by the telescope over a solid angle determined by the aperture of the telescope and the wavelength.

Appendix 1 summarizes some of the key concepts in optical and radio telescopes with the different nomenclature used at optical and radio wavelengths.

Appendix 2 is a compilation of the world's large cm radio telescopes. Only operating radio telescopes with a diameter greater than 25 m (or equivalent area) are included.

2 History

2.1 Early History

The definitive history of the development of radio astronomy from the beginnings in the 1930s up to 1953 can be found in Sullivan (2009). The new radio window on the universe was opened unexpectedly in 1932 by Jansky (1933a, b) from Bell Telephone Laboratory in the USA. Jansky detected radio emission from the Milky Way while investigating the source of noise on Trans Atlantic telephone routes. With no theoretical framework to understand these results and a vast communication gap between the astronomers and the engineers, this discovery was largely ignored until 1937 when Reber built the first parabolic dish larger than a few meters (see Reber 1958). Reber changed from the "bent wire" antennas to a 31-ft parabolic dish with amplifiers at the focus so he could work at higher frequencies (3.3 GHz) and more easily change frequency. At the time, the only concept for the source of the radio emission was thermal processes, so in this Rayleigh-Jeans region of the spectrum, it was expected that the emission detected by Jansky at 20.5 MHz (15 m) would be much more intense at cm wavelengths. This division between arrays of tuned elements at low frequencies and the more recognizable parabolic dishes at higher frequencies continues to this day.

During World War II the radio frequency technology developed rapidly due to the use of radar systems, so by 1946, the time was ripe to return to observations of the sky with far more sensitive radio equipment. Development of the equipment needed for receiving radio waves took off in many countries (UK, France, Australia, Japan, Russia, Canada, USA, see Sullivan (2009), but early developments were dominated by the groups led by Ryle at the University of Cambridge, UK, and by Pawsey at the CSIR (later CSIRO) in Sydney, Australia.

2.2 Evolution of Radio Telescope Sensitivity

2.2.1 Exponential Growth in Science

Harwit (1981) showed that the most important discoveries in astronomy result from technical innovation. The discoveries peak soon after new technology appears, and typically within 5 years of the technical capability. Instruments used for discoveries are often built by the observer. It had already been well established that most scientific advances follow technical innovation in other areas of science. de Solla Price (1963) applied quantitative measurement to the progress of science (scientometrics) and reached the conclusion that most scientific advances follow laboratory experiments. His analysis also showed that the normal mode of growth of science is exponential. A rather simplified conclusion to draw from this is that any

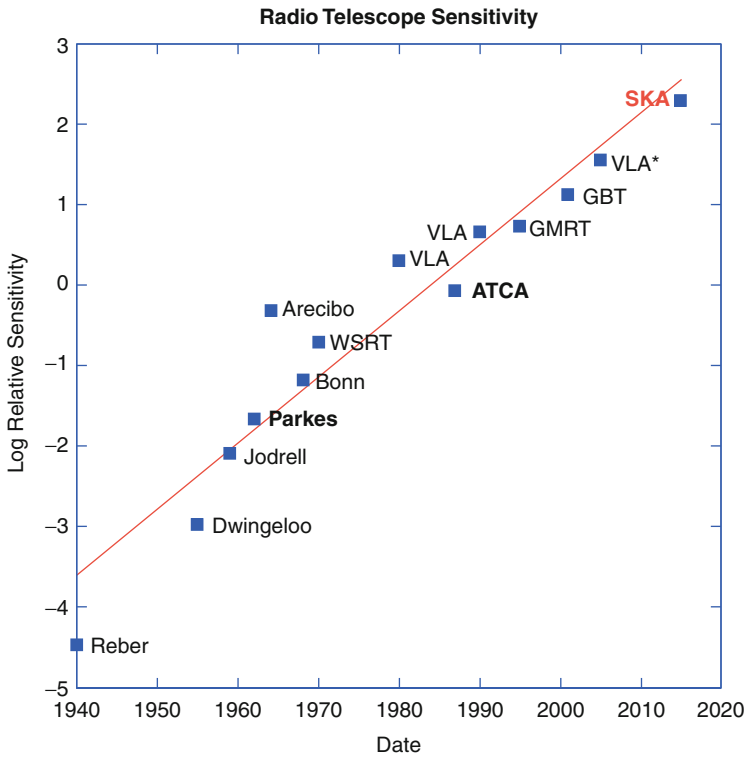

Fig. 8-1

Radio telescope sensitivity vs. time. Points are the relative continuum point source sensitivity when the telescopes were built, or after major upgrades. VLA* is the EVLA upgrade, now named the Jansky VLA. SKA is the proposed sensitivity for a telescope which has not yet been built (see Sect. 13)

field which has not maintained an exponential growth has now died out, so current active research areas are all still in an exponential growth phase. Furthermore, to maintain the exponential, the continual introduction of new technology is required since just refining existing technology plateaus out.

2.2.2 Livingston Curve

A famous example which illustrates this very well is the rate of increase of operating energy in particle accelerators by Livingston and Blewett (1962). Starting in 1930, each particle accelerator technology provided exponential growth up to a ceiling when a new technology was introduced. The envelope of the set of curves is itself an exponential with an increase in energy of 10^{10} in 60 years. This has been updated by Riesselmann (2009) to include the Large Hadron Collider. This example of exponential growth, originally presented by Fermi in 1954, has become known as the "Livingston Curve."

To this we can add the now famous "Moore's law" for computing devices (more precisely for transistors on a chip). Moore (1965) noted that the transistor density of semiconductor chips

doubled roughly every 1–2 years. This was later refined to doubling every 18 months, and this exponential growth has been maintained for the last 40 years (Mollick 2006).

Figure 8-1 plots the point source continuum sensitivity of telescopes used for radio astronomy since the first discovery of extraterrestrial radio emission in 1940. It has been exponential with an increase in sensitivity of 10^5 since 1940, doubling every 3 years. Also in this case, we can see particular radio telescope technologies reaching ceilings and new technologies being introduced, e.g., the transition from huge single dishes to arrays of smaller dishes in the 1980s.

2.3 The Development of the Aperture Synthesis Radio Telescope

Because of the long radio wavelengths, it was realized that interferometers with large spacings between the elements would be required to obtain high-enough angular resolution to determine the origin of the radio waves. Two of the main pioneering groups were at the University of Cambridge in the UK, led by Ryle, and at the CSIRO (then CSIR) Division of Radiophysics in Sydney, Australia, led by Pawsey. Both groups used the WWII radar technology to build astronomical instruments.

2.3.1 Australian Group

In Australia, the main focus was on solar imaging (see Chap. 71). The sun is a strong source but has a complex and time variable structure requiring good instantaneous measurements of the Fourier components. For this reason, the Australian arrays followed an evolutionary path with large numbers of relatively small elements.

In 1951, Christiansen built the Potts Hill grating array with thirty-two 6-ft diameter dishes near Sydney, Australia. By 1955, the first earth rotation synthesis image was obtained by Christiansen and Warburton (1955). Wild (1967) built a 3-km diameter circle of ninety-six 3-m dishes which made moving images of the radio sun. It operated for 17 years from 1967 and resolved many of the questions about the nature of solar bursts.

2.3.2 Cambridge Group

After early experiments observing the sun, Ryle's group in Cambridge moved their focus to the observation of "radio stars." These sources were static but much weaker than the sun, so the arrays evolved along a different path. They used movable antennas and earth rotation to build up the Fourier components over time, and they needed much larger elements to achieve the sensitivity required for the fainter sources. This evolution culminated in the construction of the One-Mile Telescope in 1963 (Ryle and Hewish 1960).

2.3.3 The Beginnings of Aperture Synthesis

The first published suggestion that it would be possible to synthesize an image of the radio sky by measuring a range of Fourier components was made by McCready et al. (1947). However, this technique was impractical with the cliff interferometers they were using and was not suitable for imaging solar bursts which were strongly variable in both time and frequency.

The first observations using a range of Fourier components measured with an interferometer with movable elements were made at the Cavendish Laboratory by Stanier (1950), Machin (1951), and O'Brien (1953).

2.3.4 Earth Rotation Synthesis

In June 1961, radio astronomers at the Cavendish Laboratory in Cambridge, UK, used 4C aerials operating at 178 MHz to make a radio source survey of the North Pole region using the earth's rotation to fully sample the aperture plane (Ryle and Neville 1962). Computations and graphical display used EDSACII which was the first use of a digital computer for radio astronomy imaging. The X-ray crystallographers in the Cavendish laboratory had developed the necessary Fourier transform programs. This was 7 years after Christiansen and Warburton (1955) first demonstrated the Earth's rotation synthesis with an observation of the quiet sun using an array of small dishes in Australia. However, the Australian group took many months to calculate by hand the Fourier transforms for one image, and the method was considered impractical at the time.

In 1962, the Cambridge group went on to build the One-Mile Telescope (Ryle and Hewish 1960) and the 5-km telescope in 1971. Ryle was awarded the Nobel Prize in 1974 "For his observations and inventions, in particular for the aperture synthesis technique."

The further development of Fourier imaging, deconvolution, and self-calibration will be described in Volume 2, Chap. 7.

3 Radio Astronomy Fundamentals

A summary of the basics of electromagnetic radiation that are useful for the discussions in this chapter is provided in the following section. More details and physical background are available in a number of textbooks, for example, Kraus (1986), Burke and Graham-Smith (1996), and Wilson et al. (2008).

3.1 Radiative Transfer and Black Body Radiation

The total flux of a source is obtained by integrating intensity (in $\mathrm{W\,m^{-2}\,Hz^{-1}\,sr^{-1}}$) over the total solid angle Ω_s subtended by the source

$$S_\nu = \int_{\Omega_s} I_\nu(\theta, \varphi) \cos\theta \, \mathrm{d}\Omega. \tag{8.1}$$

The flux density of an astronomical source is given in units of a jansky (Jy). The jansky was adopted by the IAU in 1973 as the unit of spectral flux density. $1\,\mathrm{Jy} = 10^{-26}\,\mathrm{W\,m^{-2}\,Hz^{-1}}$. The strongest of the (nonsolar) continuum radio sources are a few hundred jansky, and the current sensitivity limits for modern radio telescopes are now at the sub mJy level. Future telescopes such as the SKA will reach μJy sensitivity.

The spectral distribution of the radiation of a black body in thermodynamic equilibrium is given by the Planck law:

$$B_\nu(T) = \frac{2h\nu^3}{c^2}\frac{1}{e^{h\nu/kT}-1} \quad . \tag{8.2}$$

If $h\nu \ll kT$, the *Rayleigh-Jeans Law* is obtained:

$$B_{RJ}(\nu, T) = \frac{2\nu^2}{c^2}kT \quad . \tag{8.3}$$

In the Rayleigh-Jeans relation, the brightness and the thermodynamic temperatures of black body emitters are strictly proportional (8.3). This feature is useful, so the normal expression of brightness of an extended source is *brightness temperature* T_B:

$$T_B = \frac{c^2}{2k}\frac{1}{\nu^2}I_\nu = \frac{\lambda^2}{2k}I_\nu \, . \tag{8.4}$$

If I_ν is emitted by a black body and $h\nu \ll kT$, then (8.4) gives the thermodynamic temperature of the source, a value that is independent of ν. If other processes are responsible for the emission of the radiation (e.g., synchrotron, free-free, or broadband dust emission), T_B will depend on the frequency; however, (8.4) is still used.

3.2 The Nyquist Theorem and Noise Temperature

This theorem relates the thermodynamic quantity temperature to the electrical quantities voltage and power. This is essential for the analysis of noise in receiver systems. The average power per unit bandwidth, P_ν (also referred to as power spectral density, PSD), produced by a resistor R is

$$P_\nu = \langle iv \rangle = \frac{\langle v^2 \rangle}{2R} = \frac{1}{4R}\langle v_N^2 \rangle \, , \tag{8.5}$$

where $v(t)$ is the voltage that is produced by i across R, and $\langle \cdots \rangle$ indicates a time average. The first factor $\frac{1}{2}$ arises from the condition for the transfer of maximum power from R over a broad range of frequencies. The second factor $\frac{1}{2}$ arises from the time average of v^2. Then

$$\langle v_N^2 \rangle = 4R\,k\,T \, . \tag{8.6}$$

When inserted into (8.5), the result is

$$P_\nu = k\,T \, . \tag{8.7}$$

Equation 8.7 can also be obtained by a reformulation of the Planck law for one dimension in the Rayleigh-Jeans limit. Thus, the available noise power of a resistor is proportional to its temperature, the *noise temperature* T_N, independent of the value of R and of frequency.

Not all circuit elements can be characterized by thermal noise. For example, a microwave oscillator can deliver 1 μW, the equivalent of more than 10^{16} K, although the physical temperature is ~300 K. This is an example of a very *nonthermal* process, so temperature is not a useful concept in this case.

3.3 Overview of Intensity, Flux Density, and Main Beam Brightness Temperature

Temperatures in radio astronomy have given rise to some confusion. A short summary is given here. Power is measured by an instrument consisting of an antenna and a receiver. The power input can be calibrated and expressed as flux density or intensity. For very extended sources, intensity (see (8.4)) can be expressed as a temperature, the *main beam brightness temperature*, T_{MB}. For discrete sources, the combination of (8.1) with (8.4) gives

$$\boxed{S_\nu = \frac{2k}{\lambda^2}\, T_B} \quad . \tag{8.8}$$

For a source with a Gaussian spatial distribution, this relation is

$$\left[\frac{S_\nu}{\mathrm{Jy}}\right] = 0.0736\, T_B \left[\frac{\theta}{\mathrm{arcsec}}\right]^2 \left[\frac{\lambda}{\mathrm{mm}}\right]^{-2} \tag{8.9}$$

if the flux density S_ν and the actual (or "true") source size are known, then the *true brightness temperature*, T_B, of the source can be determined. For local thermodynamic equilibrium (LTE), T_B represents the physical temperature of the source. If the *apparent* source size, that is, the source angular size as measured with an antenna is known, (8.9) allows a calculation of T_{MB}. For discrete sources, T_{MB} depends on the angular resolution. If the antenna beam size has a Gaussian shape θ_b, the relation of actual θ_s and apparent size θ_o is:

$$\theta_o^2 = \theta_s^2 + \theta_b^2 \,. \tag{8.10}$$

then from (8.8), the relation of T_{MB} and T_B is

$$T_{MB}\left(\theta_s^2 + \theta_b^2\right) = T_B\, \theta_s^2 \tag{8.11}$$

Finally, the PSD entering the receiver (8.7) is antenna temperature, T_A; this is relevant for estimating signal to noise ratios (see (8.21) and (8.24)).

3.4 Polarization

Hertz dipoles are sensitive to a single linear polarization. By rotating the dipole over an angle perpendicular to the direction of the radiation, it is possible to determine the amount and angle of linearly polarized radiation. Helical antennas or arrangements of two dipoles are sensitive to circular polarization. Generally, polarized radiation is a combination of linear and circular, and is usually less than 100% polarized; so four parameters must be specified. It is usual to characterize polarization by the four Stokes parameters, which are the sum or difference of measured quantities. The total intensity of a wave is given by the parameter I. The amount and angle of linear polarization are given by the parameters Q and U, while the amount and sense of circular polarization are given by the parameter V. The definition of the sense of circular polarization in radio astronomy is the same as in electrical engineering but *opposite* to that used in the optical range; see Born and Wolf (1965) for a complete analysis of polarization, using the *optical* definition of circular polarization. Poincaré introduced a representation that permits an easy visualization of all the different states of polarization of a vector wave. See Radhakrishan (1990), Thompson et al. (2001), or Wilson et al. (2008) for more details.

3.5 Sensitivity

The noise contributions from source, atmosphere, ground, telescope surface, and receiver are always additive:

$$T_{\text{sys}} = \sum T_i \tag{8.12}$$

From Gaussian statistics, the root mean square, RMS, noise is given by the mean value divided by the square root of the number of samples. From the estimate that the number of samples is given by the product of receiver bandwidth multiplied by the integration time, the result is

$$\boxed{\Delta T_{\text{RMS}} = \frac{T_{\text{sys}}}{\sqrt{\Delta\nu\,\tau}} = \frac{(T_A + T_{RX})}{\sqrt{\Delta\nu\,\tau}}} \quad . \tag{8.13}$$

Where T_{A} represents the power entering the receiver from the antenna and includes the source, the atmosphere, and the ground and T_{RX} represents the noise power added by the receiver. At very long (m) and short (mm) wavelengths, T_{A} will dominate T_{rx}. A more detailed derivation is to be found in Wilson et al. (2008).

4 Antennas

The antenna serves to focus power into the feed, a device that efficiently transfers power in the electromagnetic wave to the receiver. According to the principle of *reciprocity*, the properties of antennas such as beam sizes, efficiencies, etc. are the same whether these are used for receiving or transmitting. Reciprocity holds in astronomy, so it is usual to interchangeably use expressions that involve either transmission or reception when discussing antenna properties. For example, the terms *beam* and *feed* come from early radar usage. All of the following applies to the far-field radiation.

4.1 The Hertz Dipole

The total power radiated from a dipole carrying an oscillating current I at a wavelength λ is

$$\boxed{P = \frac{2c}{3}\left(\frac{I\Delta l}{2\lambda}\right)^2} \quad . \tag{8.14}$$

For the dipole, the radiation is linearly polarized with the electric field along the direction of the dipole. The radiation pattern has a doughnut shape, with the cylindrically symmetric maximum perpendicular to the axis of the dipole. Along the direction of the dipole, the radiation field is zero. To improve directivity, reflecting screens have been placed behind a dipole, and in addition, collections of dipoles, driven in phase, are used. Dipole radiators have the best efficiency when the size of the dipole is $1/2\,\lambda$.

4.2 Filled Apertures

This section provides a simplified description of antenna properties. For more details, see Baars (2007). At cm and shorter wavelengths, flared waveguides ("feed horns") or dipoles are used to convey power focused by the antenna (i.e., electromagnetic waves in free space) to the receiver (voltage). At the longest wavelengths, dipoles are used as the antennas. Details are to be found in Love (1976) and Goldsmith (1988, 1994).

4.2.1 Angular Resolution and Efficiencies

From diffraction theory (see Jenkins and White 2001), the angular resolution of a reflector of diameter D at a wavelength λ is

$$\boxed{\theta = k\frac{\lambda}{D}} \quad . \tag{8.15}$$

where k is of order unity. This universal result gives a value for θ (here in radians when D and λ have the same units). Diffraction theory also predicts the unavoidable presence of sidelobes, that is, secondary maxima. The sidelobes can be reduced by *tapering* the antenna illumination. Tapering lowers the response to very compact sources and increases the value of θ, that is, widens the beam due to the effective decrease in D.

The *normalized power pattern* is:

$$\boxed{P_\mathrm{n}(\vartheta,\varphi) = \frac{1}{P_\mathrm{max}}\,P(\vartheta,\varphi)} \quad . \tag{8.16}$$

The *beam solid angle* Ω_A of an antenna is given by

$$\boxed{\Omega_\mathrm{A} = \int\limits_{4\pi}\int P_\mathrm{n}(\vartheta,\varphi)\;\mathrm{d}\Omega = \int\limits_0^{2\pi}\int\limits_0^{\pi} P_\mathrm{n}(\vartheta,\varphi)\sin\vartheta\,\mathrm{d}\vartheta\,\mathrm{d}\varphi} \tag{8.17}$$

that is measured in steradians (sr). The integration is extended over all angles; so Ω_A is the solid angle of an ideal antenna having $P_\mathrm{n} = 1$ for Ω_A and $P_\mathrm{n} = 0$ everywhere else. For most antennas, the (normalized) power pattern has much larger values for a limited range of both ϑ and φ than for the remainder; the range where Ω_A is large is the main beam of the antenna; the remainder are the sidelobes or backlobes (❯ *Fig. 8-2*).

In analogy to (❯ 8.17), the *main beam solid angle* Ω_MB is defined as

$$\boxed{\Omega_\mathrm{MB} = \int\limits_{\substack{\mathrm{main}\\ \mathrm{lobe}}}\int P_\mathrm{n}(\vartheta,\varphi)\;\mathrm{d}\Omega} \quad . \tag{8.18}$$

The quality of a single antenna depends on how well the power pattern is concentrated in the main beam. The definition of *main beam efficiency* or *beam efficiency*, η_B, is

$$\boxed{\eta_\mathrm{B} = \frac{\Omega_\mathrm{MB}}{\Omega_\mathrm{A}}} \quad . \tag{8.19}$$

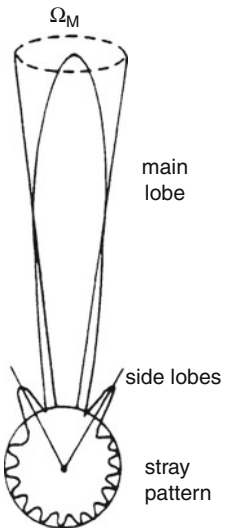

Fig. 8-2
A polar power pattern showing the main beam, and near- and farside lobes. The weaker farside lobes have been combined to form the stray pattern

η_B which is the fraction of the power is concentrated in the main beam. The main beam efficiency can be modified (within limits) for parabolic antennas by changing the illumination of the main reflector. An under-illuminated antenna has a wider main beam but lower sidelobes. The angular extent of the main beam is usually described by the *full width to half power width* (FWHP), the angle between points of the main beam where the normalized power pattern falls to 1/2 of the maximum. The beamwidth θ is given by (8.15).

If a plane wave with the power density $|\langle\vec{S}\rangle|$ in W m^{-2} is intercepted by an antenna, a certain amount of power is extracted from this wave. This power is P_e, and the fraction is

$$A_e = P_e / |\langle\vec{S}\rangle|, \tag{8.20}$$

the *effective aperture* of the antenna. A_e has the dimension of m^2. Compared to the *geometric aperture* A_g, an aperture efficiency η_A can be defined by

$$\boxed{A_e = \eta_A A_g} \quad . \tag{8.21}$$

If an antenna with a normalized power pattern $P_n(\vartheta, \varphi)$ is used to receive radiation from a brightness distribution $B_\nu(\vartheta, \varphi)$ in the sky, at the output terminals of the antenna, the power per unit bandwidth (PSD), in W Hz^{-1}, P_ν is

$$P_\nu = \tfrac{1}{2} A_e \int\int B_\nu(\vartheta, \varphi)\, P_n(\vartheta, \varphi)\, \mathrm{d}\Omega \,. \tag{8.22}$$

By definition, this operates in the Rayleigh-Jeans limit, so the equivalent distribution of brightness temperature can be replaced by an equivalent *antenna temperature* T_A (8.7):

$$P_\nu = k\, T_A \,. \tag{8.23}$$

This definition of *antenna temperature* relates the output of the antenna to the power from a matched resistor. When these two power levels are equal, then the antenna temperature is given by the temperature of the resistor. The effective aperture A_e can be replaced by the the beam solid angle $\Omega_A \cdot \lambda^2$. Then (8.22) becomes

$$\boxed{T_A(\vartheta_0, \varphi_0) = \frac{\int T_B(\vartheta, \varphi) P_n(\vartheta - \vartheta_0, \varphi - \varphi_0) \sin\vartheta \, d\vartheta \, d\varphi}{\int P_n(\vartheta, \varphi) \, d\Omega}} \tag{8.24}$$

From (8.24), $T_A < T_B$ in all cases. The numerator is the *convolution* of the brightness temperature with the beam pattern of the telescope (Fourier methods are of great value in this analysis; see Bracewell 1986). The brightness temperature $T_b(\vartheta, \varphi)$ corresponds to the thermodynamic temperature of the radiating material *only* for thermal radiation in the Rayleigh-Jeans limit from an optically thick source; in all other cases, T_B is a convenient quantity that represents source intensity at a given frequency.

For a source small compared to the beam, (8.22) and (8.23) give

$$P_\nu = \tfrac{1}{2} A_e S_\nu = k T_A \tag{8.25}$$

T_A is the antenna temperature at the receiver.

$$\boxed{T_A = \Gamma S_\nu} \tag{8.26}$$

where Γ is the *sensitivity* of the telescope measured in K Jy^{-1}. Introducing the aperture efficiency η_A according to (8.21), we find

$$\boxed{\Gamma = \eta_A \frac{\pi D^2}{8k}} \quad . \tag{8.27}$$

Thus, Γ or η_A can be measured with the help of a calibrating source provided that the diameter D and the noise power scale in the receiving system are known. When (8.26) is solved for S_ν, the result is:

$$S_\nu = 3{,}520 \, \frac{T_A(\mathrm{K})}{\eta_A (\mathrm{D/m})^2} \, . \tag{8.28}$$

4.2.2 Foci, Blockage, and Surface Accuracy

If the size of a radio telescope is more than a few hundred wavelengths, designs are similar to those of optical telescopes. Cassegrain, Gregorian, and Nasmyth systems have been used. See *Fig. 8-3* for a sketch of these focal systems. In a Cassegrain system, a convex hyperbolic reflector is introduced into the converging beam immediately in front of the prime focus. This reflector transfers the converging rays to a secondary focus which, in most practical systems, is situated close to the apex of the main dish. A Gregorian system makes use of a concave reflector with an elliptical profile. This must be positioned behind the prime focus in the diverging beam. In the Nasmyth system, this secondary focus is situated in the elevation axis of the telescope by introducing another, usually flat, mirror. The advantage of a Nasmyth system is that the receiver

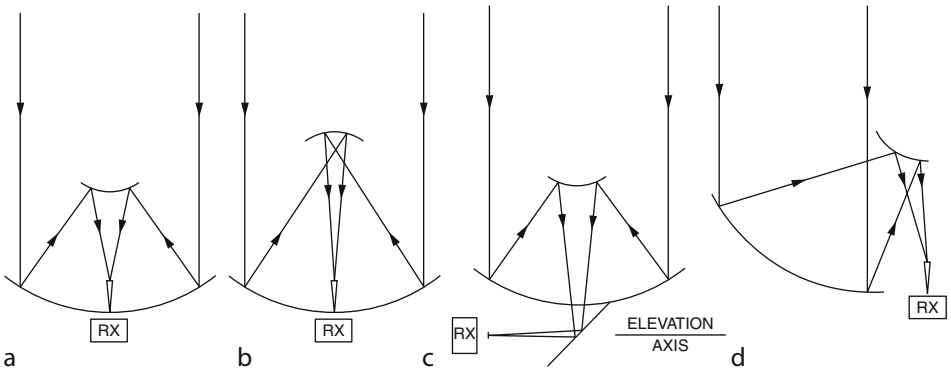

Fig. 8-3
The geometry of parabolic apertures: (a) Cassegrain, (b) Gregorian, (c) Nasmyth, and (d) offset Cassegrain systems (From Wilson et al. 2008)

front ends remain horizontal while the telescope is pointed toward different elevations. This is an advantage for receivers cooled with liquid helium, which may become unstable when tipped. Cassegrain and Nasmyth foci are commonly used in the mm/sub-mm wavelength ranges.

In a secondary reflector system, feed illumination beyond the edge receives radiation from the sky, which has a temperature of only a few K. For low-noise systems, this results in only a small overall system noise temperature. This is significantly less than for prime focus systems. This is quantified in the so-called G/T value, that is, the ratio of antenna gain to system noise. Any telescope design must aim to minimize the excess noise at the receiver input while maximizing gain. For a specific antenna, this maximization involves the design of feeds and the choice of foci.

The secondary reflector and its supports block the central parts in the main dish from reflecting the incoming radiation, causing some significant differences between the actual beam pattern and that of an unobstructed antenna. Modern designs seek to minimize blockage due to the support legs and subreflector.

Feed leg blockage will cause deviations from circular symmetry. For altitude-azimuth telescopes, these sidelobes will change position on the sky with hour angle (see Reich et al. 1978). This may be a serious defect, since these effects will be significant for maps of low-intensity regions near an intense source. The sidelobe response may depend on the polarization of the incoming radiation. Equatorially mounted telescopes avoid this problem but at high cost for a large telescope. A new option now being explored is the three axis mount so an alt-az telescope can rotate about a third axis parallel to the beam axis keeping the sidelobe patterns fixed on the sky.

The gain of a filled aperture antenna with small-scale surface irregularities ε cannot increase indefinitely with increasing frequency but reaches a maximum at $\lambda_m = 4\pi\varepsilon$, and this gain is a factor of 2.7 below that of an error-free antenna of identical dimensions. The usual rule-of-thumb is that the irregularities should be 1/16 of the shortest wavelength used.

5 Interferometers and Aperture Synthesis

From diffraction theory, the angular resolution is given by (8.15). However, as shown by Michelson (see Jenkins and White 2001), a much higher resolving power can be obtained by coherently combining the output of two reflectors of diameter $d \ll B$ separated by a distance B yielding $\theta \approx \lambda/\mathrm{B}$. In the Rayleigh-Jeans regime, $h\nu \ll kT$, the outputs can be amplified without seriously degrading the signal-to-noise ratio. This amplified signal can be divided and used to produce a large number of cross-correlations (e.g., see Radhakrishnan 1999).

The simplest case is a two-element system in which electromagnetic waves are received by two antennas. These induce the voltage V_1 at A_1:

$$V_1 \propto E\,\mathrm{e}^{\,\mathrm{i}\,\omega t}\,, \tag{8.29}$$

while at A_2:

$$V_2 \propto E\,\mathrm{e}^{\,\mathrm{i}\,\omega\,(t-\tau)}\,, \tag{8.30}$$

where E is the amplitude of the incoming electromagnetic plane wave, τ is the geometric delay caused by the relative orientation of the interferometer baseline $\vec{B}$ and the direction of the wave propagation. For simplicity, receiver noise and instrumental phase were neglected in (8.29) and (8.30). These two outputs will be correlated. Today, all radio interferometers use direct correlation followed by an integrator.

The output is proportional to

$$R(\tau) \propto \frac{E^2}{T} \int_0^T \mathrm{e}^{\,\mathrm{i}\,\omega t}\,\mathrm{e}^{\,-\mathrm{i}\,\omega(t-\tau)}\,\mathrm{d}t\,.$$

If T is a time much longer than the time of a single full oscillation, that is, $T \gg 2\pi/\omega$, then the average over time T will not differ much from the average over a single full period, resulting in

$$\boxed{R(\tau) \propto E^2\,\mathrm{e}^{\,\mathrm{i}\,\omega\tau}} \quad . \tag{8.31}$$

The output of the correlator + integrator varies periodically with τ, the delay. Since $\vec{s}$ is slowly changing due to the rotation of the earth, τ will vary, producing *interference fringes* as a function of time.

The basic components of a two-element system are shown in *Fig. 8-4*. If the radio brightness distribution is given by $I_\nu(\vec{s})$, the power received per bandwidth $\mathrm{d}\nu$ from the source element $\mathrm{d}\Omega$ is $A(\vec{s})I_\nu(\vec{s})\,\mathrm{d}\Omega\,\mathrm{d}\nu$, where $A(\vec{s})$ is the effective collecting area in the direction $\vec{s}$; the same $A(\vec{s})$ is assumed for each of the antennas. The amplifiers are assumed to have constant gain and phase factors (neglected here for simplicity).

The output of the correlator for radiation from the direction $\vec{s}$ (*Fig. 8-4*) is

$$r_{12} = A(\vec{s})\,I_\nu(\vec{s})\;\mathrm{e}^{\,\mathrm{i}\,\omega\tau}\;\mathrm{d}\Omega\,\mathrm{d}\nu \tag{8.32}$$

where τ is the difference between the geometrical and instrumental delays τ_g and τ_i. If $\vec{B}$ is the baseline vector between the two antennas

$$\tau = \tau_\mathrm{g} - \tau_\mathrm{i} = \frac{1}{c}\,\vec{B}\cdot\vec{s} - \tau_\mathrm{i}, \tag{8.33}$$

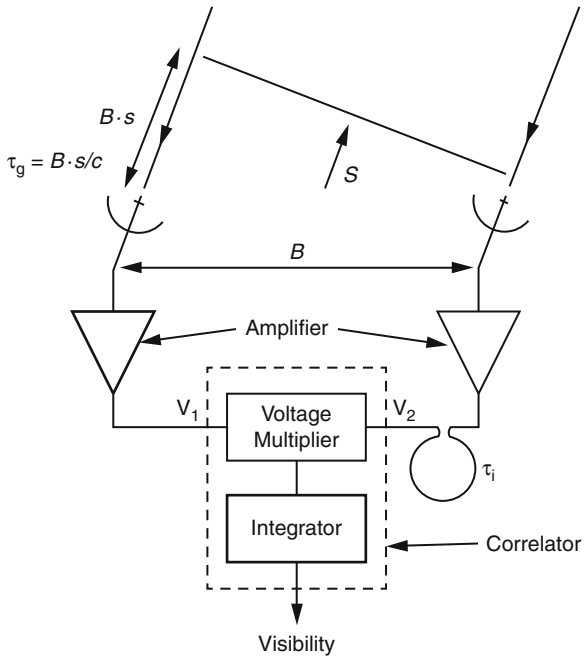

Fig. 8-4

A schematic diagram of a two-element correlation interferometer. The antenna output voltages are V_1 and V_2; the instrumental delay is τ_i and the geometric delay is τ_g. $\vec{s}$ is the direction to the source. Perpendicular to $\vec{s}$ is the projection of the baseline $\vec{B}$. The signal is digitized after conversion to an intermediate frequency. Time delays are introduced using digital shift registers (From Wilson et al. 2008)

the total response is obtained by integrating over the source S

$$R(\vec{B}) = \int\limits_{\Omega}\int A(\vec{s}) I_\nu(\vec{s})\, \mathrm{e}^{2\pi\,\mathrm{i}\,\nu\left(\frac{1}{c}\,\vec{B}\cdot\vec{s}-\tau_\mathrm{i}\right)}\,\mathrm{d}\Omega\,\mathrm{d}\nu \tag{8.34}$$

The function $R(\vec{B})$, the *Visibility Function* is closely related to the mutual coherence function (see Born and Wolf 1965; Thompson et al. 2001; Wilson et al. 2008) of the source. For parabolic antennas, it is usually assumed that $A(\vec{s}) = 0$ outside the main beam area so that (8.34) is integrated only over this region. A one-dimensional version of (8.34), for a baseline B, frequency $\nu = \nu_0$ and instrumental time delay $\tau_i = 0$, is

$$R(B) = \int A(\theta)\, I_\nu(\theta)\, \mathrm{e}^{2\pi\,\mathrm{i}\,\nu_0\left(\frac{1}{c}\,B\,\theta\right)}\,\mathrm{d}\theta, \tag{8.35}$$

With $\theta = x$ and $B_x/\lambda = u$, this is

$$R(B) = \int A(\theta)\, I_\nu(\theta)\, \mathrm{e}^{2\pi\,\mathrm{i}\,u\,x}\,\mathrm{d}\theta. \tag{8.36}$$

This form of (8.34) illustrates more clearly the Fourier transform relation of u and x.

5.1 Aperture Synthesis

To produce an image, the integral equation (8.34) must be inverted. A number of approximations may have to be applied to produce high-quality images. In addition, the data are affected by noise.

For imaging over a limited region of the sky, rectangular coordinates are adequate, so relation (8.34) can be rewritten with coordinates (x, y) in the image plane and coordinates (u, v) in the Fourier plane. The coordinate w, corresponding to the difference in height, is set to zero. Then the relevant relation is

$$I'(x,y) = A(x,y)\, I(x,y) = \int_{-\infty}^{\infty} V(u,v,0)\, \mathrm{e}^{-2\pi \mathrm{i}\,(ux+vy)}\, \mathrm{d}u\, \mathrm{d}v \tag{8.37}$$

where $I'(x, y)$ is the intensity $I(x, y)$ modified by the primary beam shape $A(x, y)$. It is easy to correct $I'(x, y)$ by dividing by $A(x, y)$.

5.2 Interferometer Sensitivity

The random noise limit to an interferometer system can be calculated following the method used for a single telescope (8.13). The use of (8.25) provides a conversion from ΔT_{RMS} to ΔS_ν. For an array of n identical antennas, there are $N = n(n-1)/2$ simultaneous pairwise correlations, so the RMS variation in flux density is

$$\Delta S_\nu = \frac{2\, M\, k\, T_{\mathrm{sys}}}{A_{\mathrm{e}} \sqrt{2\, N\, t\, \Delta\nu}}, \tag{8.38}$$

with M≅ 1, A_{e} the effective area of each antenna and T_{sys} given by (8.12). This relation can be recast in the form of brightness temperature fluctuations using the Rayleigh-Jeans relation; then the RMS noise in brightness temperature units is

$$\Delta T_{\mathrm{B}} = \frac{2\, M\, k\, \lambda^2\, T_{\mathrm{sys}}}{A_{\mathrm{e}} \Omega_{\mathrm{b}} \sqrt{2\, N\, t\, \Delta\nu}}\,. \tag{8.39}$$

For a Gaussian beam, $\Omega_{\mathrm{mb}} = 1.133\, \theta^2$, so the RMS temperature fluctuations can be related to observed properties of a synthesis image.

6 Design Criteria

Parabolic dishes are the design choice if a large collecting area is required with frequency agility. All high-frequency radio telescopes are based on the parabolic dish concept, either single dishes (Sect. 4.2) or arrays of such dishes (Sect. 7).

The advantage of the parabolic dish is the flexibility resulting from having a single receiver at the focal point. Frequency agility can then be obtained by changing the receiver system used. Such receiver changes can be made manually or with automatic systems involving rotating turrets, translators, or tilting subreflectors to move the different receivers into the focus.

However, recent developments are now changing this many decades old paradigm: Narrowband highly optimized single pixel feeds which had to be moved in and out of the focal position

to change observing frequency are being replaced by wideband feeds and receivers which cover all the required frequencies simultaneously. The single pixel feeds which observed a single point on the sky are being replaced by multibeam receivers or focal plane arrays which can use more of the information in the focal plane to image a larger area of sky (Sect. 7.5) or to observe more than one direction simultaneously as in the VERA astrometric VLBI array (Kawaguchi et al. 2000). The huge advances in digital processing have changed the balance between analog and digital, moving the transition from the aperture arrays of dipoles to the parabolic dishes to higher frequencies (Sect. 11.3).

6.1 Frequency Range

The combination of the antenna and feed which couples the electromagnetic radiation field to the amplifying receiver makes it impossible to design a single detector system that works over the entire >1,000:1 radio astronomy wavelength range. High-efficiency systems are generally constrained to an octave bandwidth, but extending this range is an active current research topic in feed design, for example, Kildal et al. (2009), Akgiray et al. (2011). Bandwidths of 10:1 are now being achieved. The advent of higher-speed digital signal processing (Sect. 11.3.1) has also made it possible to increase the backend bandwidth to many GHz so a wide range of frequency can be observed simultaneously.

6.2 Sensitivity and Survey Speed

From (8.13) and (8.25) for one polarization channel, we have

$$\Delta S_\nu = \frac{2k(T_A + T_{rx})}{A_e\sqrt{\tau\Delta\nu}}.$$

The maximum possible point source sensitivity only depends on effective aperture area (A_e), system temperature ($T_{sys} = T_A + T_{rx}$), observing time (τ), and bandwidth ($\Delta\nu$). Section 4.2.2 discussed the optimization of T_{sys} and A_e by minimizing "G/T." Further details of radio telescope receivers will be discussed in Volume 2 Chap. 6 but we note that optimized modern radio receivers in the cm bands are now close to the ultimate noise limits, and in the meter band are already well below the background noise, $T_A > T_{rx}$. Hence, the only way to further improve point source sensitivity is with more collecting area, more bandwidth, or more observation time. For spectral line observations, more bandwidth may increase the number of lines observed but cannot improve the sensitivity for any one line. It is the extreme sensitivity needed to observe the unique 21 cm H line at cosmological distances that has driven the vision of a square kilometer area array (SKA) discussed in Sect. 13.7.3. Similarly, for some transient phenomena, it is not possible to increase the observing time so again increasing collecting area is the only way forward.

For surveys, the limiting sensitivity in a given time also depends on the field of view, FoV. A survey speed figure of merit (SSFoM) can be defined which is related to the number of sources detected in a given time.

$$\text{SSFoM} \propto \text{FoV}.\Delta\nu.(A_e/T_{sys})^2 \tag{8.40}$$

where FoV = total instantaneous solid angle, $\Delta\nu$ = bandwidth, A_e = total effective area of the array, and T_{sys} = system temperature, Cordes (2007). This opens up other design opportunities as it is possible to make trade-offs between collecting area and field of view (see Sects. 6.4 and 7.5).

6.3 Angular Resolution

The struggle to obtain higher angular resolution has been the main driver since the beginning of radio astronomy. The development of all aspects of high angular resolution in radio astronomy has been reviewed by Kellermann and Moran (2001). It is ironic to note that although the long radio wavelength results in poor angular resolution, the ability to independently sample the electromagnetic field on almost unlimited baselines also gives the highest angular resolution in astronomy, see Sect. 7.8.

6.4 Field of View (FoV)

The instantaneous FoV of any radio telescope can be shown to be the product of the diffraction-limited primary beam (8.15) and the number of independent receiving elements. These receiving elements can be either in the focal or the aperture plane. The receivers might be incoherent bolometer arrays (preferred at high frequency) or coherent detectors including both multibeam receivers and phased array feeds as discussed in the next section.

7 The Antenna Arrays

The basic theory of the interferometer and an introduction to aperture synthesis is given in Sect. 5. Here we explore a number of topics which may be of interest to a broader multi-wavelength audience. There are some excellent references for the basics and for more detailed treatment, for example, Thompson et al. (2001), and Christiansen and Hogbom (1985). Further aspects of this topic are included in Chap. 7 on Radio and Optical Interferometry.

7.1 Fourier Synthesis Imaging

The theory of interferometry is straightforward: the coherence of the radiation field is measured over a large volume of space and an image formed by Fourier inversion. The practical problems of measuring the coherence from telescopes confined to the earth's surface are numerous but not too onerous. A very useful collection of practical lectures on modern aperture synthesis techniques can be found in the NRAO Summer School, Taylor et al. (1999).

The radiation can be conveniently collected using parabolic reflectors with typical diameters at centimeter wavelengths in the range 5–100 m, a diameter of 25 m being a popular compromise between cost of construction and sensitivity. Both the ability to point the antennas and the surface accuracy limit the highest practicable observing frequency.

Once the signals have been collected and amplified, they must be relayed to a central location where they are correlated with each other to form estimates of the coherence function (Sect. 5). Direct digital correlation is almost universally preferred for the flexibility and

lower levels of systematic error. Before the correlation is performed, the signals must be lined up to eliminate the continually changing geometric delay of one antenna relative to the other due to the earth's rotation. This process is analogous to tracking of a celestial object by continually tilting an optical telescope as the earth rotates. For digitized signals, the delaying is conveniently performed using large digital buffers of high-speed memory. This earth rotation complicates matters somewhat. First, a given pair of antennas, as seen from the object, rotates around in the aperture plane, smearing out fine structure in the coherence function unless the integration time is short enough. The integration timescale in which the visibility is smeared is simply related to the time it takes for earth rotation to move the most distant antenna by its diameter. For a 25 m antenna at tens of kilometers baseline, this is about 10 s. Second, the relative motion between the antennas introduces a differential Doppler shift in the radiation received, which must be canceled before correlation.

High-quality imaging required good sampling of the coherence across the aperture plane. The largest separation of the antennas fixes the highest resolution possible, while the distribution of the samples over the aperture plane determines the complexity of structure that can be imaged. While the goal is to obtain the densest possible coverage of the aperture plane, the finite number of observed correlations and the desire for high angular resolution usually results in a compromise with incomplete sampling and higher sidelobes in the synthesis image. A detailed description of the range of deconvolution algorithms which correct for the nonuniform or incomplete sampling of the aperture plane is included in ❯ Chap. 7 on Radio and Optical Interferometry and in Volume 2 ❯ Chap. 6 on Techniques of Radio Astronomy.

The coherence measurements can be made at any time over the interval while the structure has not changed. This is of course the requirement for earth rotation synthesis, and it also makes it possible to build up samples of coherence at different spacings by moving the array elements. This is essential to obtain dense coverage of the aperture plane and high resolution with a small number of elements. Many aperture synthesis arrays have some, or all, antennas moveble (VLA, WSRT, ATCA in ❯ Sect. 12).

7.2 Crosses, Ts, and Other 2D Aperture Arrays

The list of large cm radio telescopes in Table A2 includes many crosses and T-shaped aperture arrays. Ryle (1952) first pointed out that an effective gain in resolving power can be obtained with an interferometer consisting of two dissimilar primary antennaes, for example, one with a narrow beam in the east-west direction and the other with a narrow beam in the north-south direction. The next logical step was made by Mills and Little (1953), who proposed that if the two elements had a common electrical and physical center (virtually an interferometer with separations down to zero spacing), a pencil beam antenna would result. Such an antenna is known as a Mills Cross. To minimize cost, simple collinear feed systems with fixed lengths from each element to the receiver were used but this greatly restricts the band width.

This design produced a high-quality pencil beam and could be implemented with all analog components, requiring minimal digital signal processing and no Fourier transform calculations. By the 1990s, digital technology had made this approach unattractive, and some of the old crosses and Ts were modified to incorporate the more flexible digital technology (e.g., Large et al. 1994). New array designs such as VLA (❯ Sect. 12.1), GMRT (❯ Sect. 12.11), ASKAP (❯ Sect. 13.7.2), and MEERKAT (❯ Sect. 13.7.1) use nonuniform 2D antenna element distributions to measure the maximum number of Fourier components with the minimum number of elements (minimum redundancy arrays) instead of the cross or T geometry. However, the VLA

still uses linear structures, the arms of the Y, to simplify antenna movement. In a recent twist, the computer processing and I/O requirements have become so extreme that telescope designs are again being proposed with geometrical arrangements of elements which minimize the computational load, for example, Tegmark and Zaldarriaga (2010) propose a regular antenna grid for optimum use of the fast Fourier transform, and Bunton (2011) proposes redundant geometries to decrease computer load.

7.3 Phased Array Beamforming

The traditional phased arrays formed a single beam by electronically adjusting the phases of all the elements to correspond to a given pointing direction. This is still the preferred telescope design at low frequencies because the effective area of a single antenna element, such as a simple dipole is $\sim \lambda^2$ so is large at long wavelengths, and the cost per element is low. Hence, sparse-phased arrays are a very cost-effective way to obtain a large collecting area at very low frequency. However, if only a single-phased array beam is formed, the advantage of the wide FoV of each element of the array is lost and the survey speed is greatly reduced. Since we are in the Rayleigh-Jeans regime with many photons per state in the system, for example, see Radhakrishnan (1999), we can split the signal without any loss in S/N to form multiple beams pointing in different directions. It is then theoretically possible to form enough simultaneous beams to cover the whole FoV of each element. However, the number of beams needed scales as $n = A_{tot}/\lambda^2$ for an n element array of total geometrical area A_{tot}. The inputs to the electronic beamformer will also scale with n, so some of the electronics is scaling as $n^2\ (A_{tot} / \lambda^2)^2$. For 1 km^2 array at 1 m, this is a factor of 10^{12} which is well beyond even Moore's law extrapolation and beyond viable power consumption limits. The solution to this dilemma is to introduce hierarchical beamforming which allows a smooth trade-off between the number of beams, and hence electronics cost, and the areas of sky imaged simultaneously. In an array with hierarchical beam formation such as LOFAR (Sect. 13.3), groups of elements, referred to as tiles, are combined to form the *tile beam*, groups of tiles in one geographic location are then combined to form one or more *station beams* and the stations are finally combined using the normal cross-correlating techniques of aperture synthesis to form a *synthesized beam*. Hence, an observation with LOFAR will have a tile beam (roughly equivalent to the *primary beam* of an array of single dishes), a number of *station beams* which can be simultaneously pointing to different regions in the *tile beam*, and finally a Fourier transform image for the FoV of each *station beam* with the resolution of the *synthesized beam*.

Hierarchical beamforming in phased arrays is used to reduce the FoV and information data rate to a manageble level. In this process, it is possible to replace parts of the digital hierarchy with analog beamforming, and the cylinders and phased array feeds in dishes discussed in the next two sections are two examples.

7.4 Cylindrical Reflectors

Another method of reducing the FoV is to place a one-dimensional phased array at the focus of a parabolic cylindrical reflector. For a given collecting area, the reduction in the number of inputs to the beamformer is reduced by the factor lambda/2D where D is the width of the cylindrical reflector. Typically, this is a factor of 0.1–0.01 allowing the cylinders to operate at

higher frequencies than phased arrays for the same electronics cost. The advantage of the cylinder over a dish is the fact that the reflector is much cheaper, and this made the approach popular in the 1960s. However, the number of feed elements in one-dimensional phased arrays make cylindrical reflectors hard to upgrade and they were gradually displaced by the dishes.

7.5 Phased Array Feeds

There is an exact analogy between phased array beamforming in the aperture plane and the phased array feeds (PAFs) which can be placed in (or near) the focal plane of a single dish. The great advantage of putting the PAFs at the focus of a single dish is to reduce the number of active elements while retaining the sensitivity corresponding to the area of the dish. The next logical step is to place arrays of feeds in the focal plane of each dish in an interferometer array to image many fields at once. First suggested by Fisher and Bradley (2000) and now being implemented in Westerbork (APERTIF) based on an array of Vivaldi feeds (Oosterloo et al. 2010) and in ASKAP based on a self-complimentary checker board antenna using a connected patch array (Hay et al. 2008). Note that for the same FoVm the electronics' cost advantage of the PAF over the arrays is area PAF/area dish which is in the range 0.01–0.001 for current designs.

The PAF can be placed at any location along the wavefront as long as the complex distribution of amplitude of the electromagnetic wave is fully sampled. The PAF does not have to be in the focal plane, but as long as it is in a region where the wavefront has a small waist, the number of receptor elements needed is minimized.

PAFs are also referred to as focal plane arrays (FPA). The terminology PAF is preferred for arrays of elements which are combined to form phased array beams. The term FPA would refer to any array of receiving elements in the focal plane, including multibeam receivers which do not sample the focal plane continuously and bolometer detector arrays which produce separate total power beams for each element. The term "smart feeds" is also used for feeds which are electronically configurable.

7.6 Mosaicing

When a number of interferometric imaging observations are made with overlapping primary beams to cover a larger area of the sky, this is called a mosaic. Mosaicing has two benefits; obviously, the area of sky observed is now larger than the primary beam, but more subtly, additional Fourier components of the sky brightness distribution have been measured (Ekers and Rots 1979). To see how this is possible, first consider a single pointing made with a filled aperture. All the Fourier components, from the area of sky in its primary beam, are combined into a single value with weights determined by the illumination of the aperture (taper). If two dishes form an interferometer all the Fourier components corresponding to all possible pairs of elements between the two apertures are combined into a single complex visibility, that is, for two dishes of diameter D, separated by a baseline B, the resulting visibility is the average of baselines from B – D to B + D. By combining two interferometer observations with different pointings with overlapping primary beams, all the Fourier components from B – D to B + D are recovered. This is particularly powerful when B is ≈D because the recorded baselines from 0 to 2D are the "missing" short spacings that plague interferometric observations of large sources. A simple way to see how this works is to consider the two different pointings as two different phase gradients

across the aperture of the dishes. These known phase gradients make it possible to disentangle the combined Fourier components. Cornwell (1988) and Cornwell et al. (1993) demonstrate how the image deconvolution algorithms can be modified to incorporate the additional information measured in a mosaiced observation. Methods using both the linear combination of overlapping primary beams and the joint deconvolution of overlapping primary beams are now in routine use.

A new and exciting development is the combination of the use of phased array feeds in each element of the interferometer array. Now the overlapping mosaiced fields are all measured simultaneously, greatly increasing the instantaneous FoV but also reducing the effect of some errors caused by the changing atmosphere or single dish pointing, which accumulate in sequential observations of a mosaiced area.

Mosaicing becomes especially important at higher frequencies when the primary beam of the larger and more sensitive telescopes is relatively narrow. For a more detailed treatment of mosaicing, see Sect. 11.6 in Thompson et al. (2001).

7.7 Rotation Measure Synthesis

The birefringence of the magnetized plasma in interstellar and intergalactic space causes the observed linear polarization properties of radio sources to be strongly frequency-dependent. This Faraday rotation causes the position angle of the linear polarization vector to increase by an amount $\mathrm{RM}.\lambda^2$ where the magnitude of the rotation measure (RM) ranges between 10 rad m^{-2} for typical sources observed through the interstellar medium of our Galaxy and 5×10^5 rad m^{-2} for the compact radio source at the center of the Milky Way. Observations made over a large frequency range will average out all the linear polarization, unless the spectral resolution is fine enough that Faraday rotation does not cause appreciable rotation of the polarization vector across individual spectral channels (bandwidth smearing). However, the signal-to-noise ratio of the polarization measurement in each spectral channel may be too low to compute the polarization vector. The technique of rotation measure (RM) synthesis has been developed, for example, Brentjens and de Bruyn (2005), to simultaneously utilize the measurements across an entire wide frequency band and is the optimum method to extract polarization information from noisy data Macquart et al. (2012).

7.8 Long Baseline Interferometry

In 1967, a new technique of interferometry was developed in which the receiving elements were separated by such a large distance that it was necessary to operate them independently with no real-time communications link. This was accomplished by recording the undetected voltages from each site on magnetic tape timed using independent atomic clocks sufficiently accurate to maintain coherence. Later, this data is cross-correlated at a central processing station. The technique is called very long baseline interferometry (VLBI). The principles involved in VLBI are fundamentally the same as those involved in interferometers with connected elements (Thompson et al. 2001). We are now seeing a convergence of VLBI and connected arrays as the independent tape recorders are being replaced by wideband fiber optic communications links, and it is now also technically possible to maintain phase coherence with stabilized optical links.

8 The Fundamental Differences Between Arrays and Dishes

8.1 Filling Factor

A filled aperture telescope measures all Fourier components up to its maximum diameter and has brightness sensitivity which is independent of diameter. An array has a filling factor, η, which is less than 1. The brightness sensitivity of the array is decreased, and the power in its sidelobe increased by $1/\eta$. The array may still measure all Fourier components up to its maximum spacing and consequently have relatively low sidelobes even though η is less than 1 because the number of redundant spacings can be minimized. However, high angular resolution arrays will often have η much less than 1 and incomplete coverage of Fourier components with higher sidelobes and lower brightness sensitivity.

8.2 Analog Beam Formation in the Focal Plane

A conventional radio telescope at shorter wavelengths, for example, single parabolic dish with a conventional focal plane, will form a beam when the signals reflected from all the apertures are combined at a point in the focal plane before amplification and detection. The parabolic shape of the dish surface ensures that all signals from the pointing direction are combined in phase. In an array, the undetected receiver voltage outputs from each element are sampled and stored before they are later combined with appropriate delay and phase for each direction in the sky. This corresponds to the Fourier transform operation as described in ❯ Sects. 5 and ❯ 7.1, and an aperture array is normally performed in a digital computer.

8.3 Equivalence of Dishes and Arrays

Consider a single parabolic dish of diameter, d, focusing radiation from a given direction in the sky at a point in the focal plane. The surface of the dish can be divided into n contiguous sub elements of area $A_i = A_{tot}/n$. The parabolic shape of the dish ensures that the path length to the focus will be the same for radio waves reflected from each element of the aperture. Now replace each aperture element by a small dish and receiver system which samples and amplifies the voltage averaged over the same area A_i. The voltages from all these sub elements, V_i, can then be added in the phase (either in real time or later in a computer) to produce the same signal that would be received at the focus of the single dish. It can then be detected $(\sum V_i)^2$ to obtain the power from the direction in which the dish is pointing. Now if we move all the sub elements off the parabolic surface along the direction of the received wave, we can more conveniently locate them on a plane (e.g., along the ground) provided we compensate for the extra path length by adding the appropriate delay to each sub element before adding the signals. We have now formed a "phased array" as discussed in ❯ Sect. 7.3 – see, for example, Christiansen and Hogbom (1985). If the signal is monochromatic, the change in delay (which is a function of the pointing position in the sky) can be replaced by a change in phase. If the signal is not monochromatic, this change in phase will only be correct for a small region of sky around the pointing direction (called the phase center for an array); the region with no bandwidth de-correlation is called the delay beam. The signals from the sub aperture are only averaged over an area A_{tot}/n so the phased array has a much larger primary beam than the full dish. Note that the signals

formed by this phased aperture with n elements of area A_{tot}/n is identical to that of the single aperture of area A_{tot} so the S/N estimated for the single dish (Sect. 6.2) applies to a phased array with the same area.

Now consider the radiation received at a nearby point in the focal plane of the single dish or equivalently the radiation received if the pointing of the dish is changed by $\Delta\theta$. For the signals from the sub elements, this is equivalent to changing all the delays by B. cos ($\Delta\theta$) where B is the distance from the center of the dish/array. We can now form multiple beams pointing in different directions in the sky by combining the signals with the appropriate delays.

The detected power from the sum of all the sub elements is

$$\left(\sum V_i\right)^2 = \sum (V_i)^2 + \sum (V_i \,.\, V_j).$$

The first term is just the sum of self-correlations which are the total power from each element, and the second term is the sum of all possible cross-correlations between the elements. The sum of all the self-correlations includes all the emission from the sky, the atmosphere, and the ground, but these are uncorrelated between elements so do not influence the cross-correlations. Only the signal from the astronomical source will be correlated. The self-correlation term can be quite large and will be affected by gain variations in the system and variability in the radiation received from the atmosphere and the ground, making it hard to detect weak astronomical signals. It was this component that Ryle and Vonberg (1946) removed from the interferometer response when they invented the phase switch. The result is equivalent to the modern correlation interferometer array in which only the product terms are measured, either by analog or digital means.

8.4 Array Sensitivity

The previous section demonstrated the equivalence between dishes and arrays and can be used to obtain a simple sensitivity comparison. The sensitivity of the single dish is

$$\Delta S = \frac{2KT_{sys}}{A_{tot}\sqrt{\tau\Delta\nu}} = \frac{2kT_{sys}}{A_i\sqrt{n^2\tau\Delta\nu}}$$

where A_i is the area of each element. The removal of the n independent auto-correlations reduces the sensitivity of the array from n^2 independent measurements to n(n−1) measurements so the sensitivity for a correlation array of total area $A_{tot} = nA_i$ is

$$\Delta S = \frac{2KT_{sys}}{A_i\sqrt{n(n-1)\tau\Delta\nu}}.$$

For a more formal derivation of the sensitivity, see, for example, Thompson et al. (2001).

Hence, we see that the sensitivity of an array approaches the sensitivity of a single dish of the same area for large n. For a point source, all cross-correlations in the array have the same S/N, so the sensitivity is independent of the element separation, and the equivalence to a single dish of the same area applies to a correlation interferometer array of any configuration. However, if the source is resolved on some baselines, the S/N will be reduced in a complex manner which will depend on the array configuration and the source structure. In this situation, it is often necessary to estimate the resulting S/N using simulations. However, a simple estimate of the approximate sensitivity to an extended source can be obtained by estimating the total area of those array elements which are close enough to not resolve the source.

9 Backends, Data Analysis, and Software

Backends, data analysis, and software are discussed in application and data reduction/analysis methods in T.L. Wilson, Volume 2, Chap. 6, Sects. 9.1–9.5.

10 Types of Radio Frequency Interference (RFI) and Mitigation Strategies

At present, 1–2% of the spectrum in the meter and centimeter bands is protected for passive uses, such as radio astronomy. These regulations are coordinated by the International Telecommunications Union (ITU) and implemented by national regulations. However, future telescopes like the SKA and JVLA will have sensitivities up to 100 times greater than present sensitivities and bandwidths far exceeding the few percent covered by regulation. There are also experiments (e.g., the epoch of re-ionization, redshifted hydrogen in galaxies, or various molecular lines) which require access to arbitrary parts of the spectrum. Other experiments require very large bandwidths for sensitivity, spectropolarimetry, or spectral line information. The current regulations alone will not provide the necessary protection against RFI, so we need technology and radio quiet sites as well as regulation (Ekers and Bell 2002). See Ellingson (2005) and Kesteven (2010) for a more recent compilation of RFI mitigation strategies.

10.1 Radio Frequency Interference (RFI)

Interference may be naturally occurring or human-generated. Examples of naturally occurring interference include the following: spill-over, sun, lightening, meteors. Human-generated interference may come from broadcast services (e.g., TV, radio), voice and data communications (e.g., mobile telephones, two-way radio, wireless IT networks), navigation systems (e.g., GPS, GLONASS, Galileo), radar, remote sensing, electric fences, car ignitions, and domestic appliances (e.g., microwave ovens, Goris 1998).

Undesired interfering signals and astronomy signals can differ (be orthogonal) in a range of parameters, including frequency, time, position, polarization, distance, coding, positivity, and multipath. It is extremely rare that interfering and astronomy signals do not possess some level of orthogonality in this >8-dimensional parameter space. Signal processing systems are being developed to take advantage of the orthogonality and separate the astronomy signals from the RFI signals.

External interference may arise from fixed or moving sources. Not all methods of mitigation apply to both, and methods that work well for fixed sources may not work at all for moving sources.

10.2 RFI Mitigation Methods

There is no silver bullet for detecting weak astronomical signals in the presence of strong undesired RFI. A/D converters must be fast enough to give sufficient bandwidth, with a sufficient number of bits so that both strong and weak signals are well sampled. There are a range of

techniques that can make passive use of other bands possible, and, in general, these need to be used in a progressive or hierarchical way.

- *Remove at source* is obviously best, but may not be possible.
- *Regulation* providing radio quiet frequencies or regions.
- *Farside lobes* of primary and secondary elements must be both minimized and well characterized.
- *High dynamic range linear receivers* to allow appropriate detection of both astronomy (signals below the noise) and interfering signals (with peaks in some frequencies ≫ noise).
- *Notch filters* (analog, digital, or photonic) to excise bad spectral regions; if the RFI is strong, this may require *Front-end filtering* (possibly using high-temperature super conductors) to remove strong signals as soon as they enter the signal path.
- *Clip* samples from time-based data streams to mitigate burst type interference.
- *Decoding* to remove multiplexed signals. Blanking of period or time dependent signals is a very successful but simple case of this more general approach.
- *Cancelation* of undesired signals, before correlation using adaptive filters (Barnbaum and Bradley 1998).
- *Post-correlation cancelation* of undesired signals, taking advantage of phase closure techniques (Briggs et al. 2000).
- *Parametric techniques* allow the possibility of taking advantage of known interference characteristics to excise it (Ellingson et al. 2001; Athreya 2009).
- *Adaptive beamforming* to steer spatial nulls onto interfering sources. Conceptually, this is equivalent to cancelation, but it provides a way of taking advantage of the spatial orthogonallity of astronomy and interfering signals (see next section).

10.3 Adaptive Beam Nulling

This is a promising new approach and is applicable to arrays in either the aperture or focal plane, for example, Nagel et al. (2007). A physical interpretation of why you can form nulls without wrecking the synthesized beam might go as follows: Big arrays, once phased up to point in a given direction, have lots of far sidelobe nulls, which are all over the place once you get a reasonable distance from the main beam. Imagine changing the coefficients a little to get the closest null onto an interferer. Very little variation in the coefficients is required. Since the difference is so small, the main beam is hardly affected. The other nulls will shift around, of course, because they are sensitive to small changes in the coefficients.

11 General Discussion

11.1 Open Skies Policy in Radio Astronomy

Almost all radio observatories operate with an "open sky" model in which access is not limited to scientists from country or organization that operates the telescope.

This is usually justified on the basis that it guarantees the best science with the facility, whereas guaranteed access rights for scientists from funding nations favors the individual scientists more than the funding nations. The facility will still get the recognition regardless of

the nationality of the user, and with an open skies policy, it is easier to set up the large teams conducting surveys which can be made available to the entire community.

There are national benefits for financial participation in an observatory other than preferential access. These include representation in policy setting committees, involvement in future instrumental developments, and representation in time allocation committees.

11.2 Selecting the Best Telescope for Your Experiment

Given the "open skies" policy at many radio astronomy observatories, it makes sense to think about the best radio telescope for your experiment. The main decision will depend on the same telescope design criteria discussed in Sect. 6. To these, you need to add geographic location and adequate sky coverage to see your source. If you need to make an image, there may be additional declination constraints, depending on the geometry of the array. For time-variable phenomena, you may also need to observe at a specific time and hence geographic longitude. Some telescopes are optimized for imaging (usually the arrays) and others for time domain astronomy (usually the single dishes).

Selecting the right frequency will depend on the scientific requirements. If specific rest frame line transitions are involved (possibly with red shifts), the observing frequency will be obvious. Note that modern correlation spectrometers and some telescope systems support more than one simultaneous frequency band, but there are usually telescope-specific constraints which still need to be considered.

Radio continuum observations are either thermal or nonthermal. If thermal, the frequency choice will depend on the optical depth with higher frequencies required for regions with significant optical depth. For nonthermal sources at low frequencies (<1 GHz), you need to consider the S/N balance between the spectrum of the sources and the background (nonthermal) noise. If polarization information is required, you will have a complex trade-off between depolarization effects favoring higher frequencies and Faraday rotation measure sensitively favoring the lower frequencies and large fractional bandwidths.

Perhaps the most critical of the other factors are the angular resolution and field of view. Angular resolution varies by a factor of 10^5 (hence 10^{10} in brightness sensitivity). Single dishes and low frequency arrays have low-resolution and high-brightness sensitivity. The current mainstream-connected arrays (VLA, GMRT, ATCA, and WSRT) have a resolution in $0''.1$–$10''$ range and are very good when comparing with images at other wavelengths. Very high-resolution (VLBI) observations are more specialized and usually involve a very small FoV due to data transfer and processing limits.

11.3 Analog Versus Digital

This has always separated different telescope designs. In the beginning, the aperture synthesis had to wait for the computational capability to calculate Fourier transforms, and later fast Fourier transforms (Cooley and Tukey 1965). Before that, analog beamforming was the only solution. Over time, the arrays have increasingly relied on digital processing, while the single dishes used analog systems up to the final data analysis stage.

The digital vs. analog divide as a function of processing speed has evolved dramatically over time. Digital processing speed has been following Moore's law, but most analog developments

have been much slower so the transition between analog and digital has been moving to higher frequencies and wider bandwidths. Despite these changes, the digital analog divide is still with us because the bandwidths and maximum frequencies in radio telescopes still push the maximum achievable digital signal processing limits. Currently, the digital-analog transition is in the 100 GHz range for most arrays, but for very large arrays such as SKA, the number of elements still makes fully digital difficult even at a few GHz. At high frequency, the balance shifts to larger dish size due to the increased cost contribution of the very low-noise cryogenic receivers and the cost of digital signal processing bandwidth.

In addition to these general design issues, we have also had the movement of the digital/analog transition closer and closer to the front end of the system, ultimately resulting in the digital receiver.

11.3.1 Fully Digital Receivers

In a digital receiver, the whole analog radio frequency band from the output of the low-noise amplifier is digitized directly without any prior down-conversion and analog processing. All signal processing operations are performed in the digital domain, and the digital sampler (clock) replaces the local oscillator in a conventional receiver. This is also known as a software radio. The digital receiver revolution has been dramatic and has huge impact for wireless communications. For example, see Reed (2002).

These digital receivers are extremely flexible, and production costs are low. Once designed and manufactured, they are simpler to use and replicate because there is no need to tune or match various analog components. In a digital receiver, it is also easier to implement specialized real-time signal processing techniques such as RFI suppression, programmable de-dispersion, and real-time time-domain processing.

For radio astronomy applications, the digital receivers present some special challenges which are now being overcome with modern technology. High performance and stability are required, and self-generated interference produced close to the high-gain amplifiers has to be suppressed. High bandwidths are required, but multibit samplers with up to 30 GHz clock rates are now commercially available.

11.4 General Purpose Versus Specialized Telescope Designs

This debate is still as vigorous as ever involving the cost trade-offs between specialized vs. flexible general use telescopes.

The beginning of radio astronomy provides excellent examples of discoveries made by exploring the unknown (Kellermann et al. 2009). Wilkinson et al. (2004) included a tabulation of the key discoveries in radio astronomy since the beginning of the field in 1933 to 2000. *Figure 8-5a* plots these discoveries against time, comparing the discoveries made with special purpose instruments with those made on the larger general user facilities. It is clear that the number of discoveries made with special purpose instruments has declined with time. *Figure 8-5b* shows that serendipitous discoveries are also more prevalent at the inception of a new branch of science.

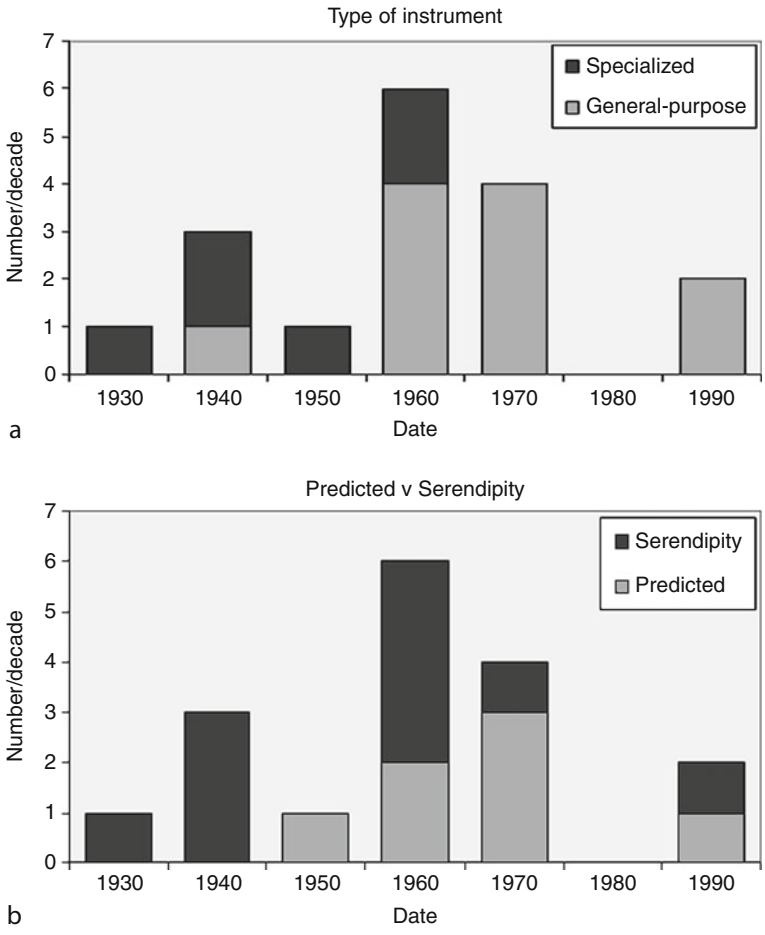

Fig. 8-5
Key discoveries in radio astronomy (From Wilkinson et al. (2004))

12 The World's Major Radio Telescopes

It is not practical to describe all the telescopes listed in Table A2, so this section is restricted to the subset of telescopes which have had the most impact based on the bibliometric analysis of Trimble and Ceja (2010).

12.1 Very Large Array (VLA, Now JVLA)

In 1965, a proposal to construct the VLA (*Fig. 8-6*) was submitted to the US National Science Foundation (NSF). With twenty-seven 25-m dishes and reconfigurable baselines in a 2D Y-shaped array extending to 36 km, this was a huge step forward in sensitivity and angular resolution (Napier et al. 1983). The antennas are Cassegrain, and the receivers are in a ring at the

Fig. 8-6
VLA with rainbow 1985 (© Doug.Johnson/Science Photo Library)

secondary focus where they can be quickly changed by a tilting 2.3-m subreflector. The 2D array provides good-quality imaging from the North Pole down to declinations of ~−40°. The four configurations give a wide range of resolution and brightness sensitivity. This was one of the first centimeter synthesis telescopes to provide good-quality imaging of equatorial sources.

The VLA construction commenced in 1972, and it was formally inaugurated in 1980. The VLA has been the most productive ground-based telescope ever built at any wavelength in both its number of publications and number of citations. The VLA sensitivity and imaging quality open radio wavelength observations to many fields of astronomy including stellar (mass loss rates), planets, Galactic variables, Galactic Center, and normal galaxies as well as the expected radio galaxy and quasar research. It is now undergoing a major upgrade (see ❯ Sect. 13.1) and will have almost complete frequency coverage with multiple low-noise dual polarization receivers from 1 to 40 GHz.

The JVLA is operated by NRAO as a National Science Foundation facility with open sky access policy.

12.2 Australia Telescope Compact Array (ATCA)

The Australian Telescope Compact Array (ATCA) started operating in 1987. It has six 22-m movable dishes and a 6-km E–W baseline. It is the premier southern hemisphere aperture synthesis telescope (Frater et al. 1992). Although it has only modest collecting area, it has multiple simultaneous frequencies and dual polarization low-noise receivers extending up to 100 GHz, very high (8 GHz) bandwidth, and low system temperature (Wilson et al. 2011).

Like the JVLA (see ❯ Sect. 13.1), it illustrates the degree to which technology development has enhanced radio telescope performance. All receivers are on a turret at the secondary focus which is rotated to bring the active receiver on-axis, resulting in exceptional polarization

performance. The long baselines are on an E–W rail track limiting good 2D imaging to declinations less than −20°. However, there are short (200-m) N–S baselines which provide lower-resolution 2D arrays which are especially useful for synthesis imaging at short wavelengths even near the equator. The ATCA was completed just in time to image the nonthermal radio emission of the SN1987a in the Magellanic Clouds and has continued to follow the development of the expanding shell for the last 25 years (Zanardo et al. 2010).

The ATCA is operated by CSIRO as a national facility with open sky access policy.

12.3 VLBA (Very Long Baseline Array)

The VLBA is a system of ten 25-m diameter parabolic dishes which was dedicated in 1993. With antennas distributed from Mauna Kea on the Big Island of Hawaii to St. Croix in the US Virgin Islands, the VLBA spans 8,000 km and provides the highest angular resolution of any telescope on Earth or in space.

The first and one of the very few confirmed super massive black holes was found in the galaxy NGC4258. Its mass and small size is traced by VLBA observations of a H_2O maser source in its nucleus (Miyoshi et al. 1995). In 1999, follow-up VLBA observation (Herrnstein et al. 1999) made the first direct extragalactic geometric distance measurement.

The VLBA is operated by NRAO as a US National Science Foundation facility and has had an open sky access policy.

12.4 MERLIN (Multi-element Radio Linked Interferomer Network)

The Multi-Element Radio Linked Interferometer Network (MERLIN) is an array of radio telescopes spread across the UK. The array consists of up to seven radio telescopes and includes the Lovell Telescope, Mark II, Cambridge, Defford, Knockin, Darnhall, and Pickmere. The longest baseline is 217 km, and MERLIN operates at frequencies between 151 MHz and 24 GHz. It was originally connected in real time using microwave radio links which have now been replaced by wideband optical fiber links.

MERLIN is operated from Jodrell Bank on behalf of the Science and Technology Facilities Council as a National Facility.

12.5 Parkes

In 1960, the CSIRO Radiophysics group in Australia built a 210-ft parabolic dish now known as the Parkes 64-m radio telescope. The aerial cabin at the prime focus houses feeds and receiver equipment. The feed platform translator at the base of the aerial cabin holds up to four receivers. The translator has remotely controled motion both up/down for focus and lateral/ rotational movement for receiver changes and polarization measurement. The alt-az mounted dish is limited in zenith angle to 59.5°.

The Parkes 21-cm Multibeam Receiver consists of a 13-beam cooled dual polarization 21-cm receiver system located at the prime focus of the 64-m dish. This receiver has had huge impact for pulsar and HI surveys and was the forerunner for multibeam receivers now available on many radio telescopes (*Fig. 8-7*).

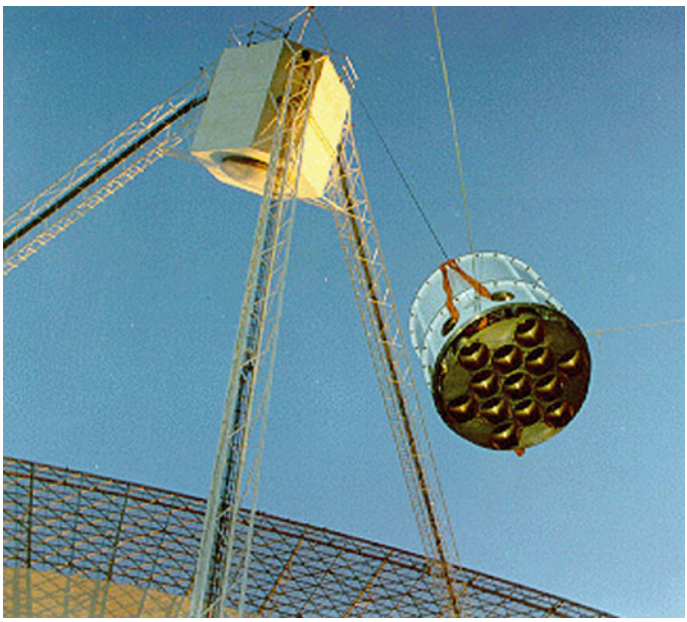

Fig. 8-7
Installation of the multibeam receiver on the Parkes radio telescope in 1997

One of the most famous observations of the CSIRO's Parkes Observatory made soon after its completion was the Lunar Occultation of 3C273 by Hazard et al. (1963) which leads to the discovery of quasars. The occultation showed an unresolved flat-spectrum core and a 20″ steeper spectrum jet structure. The morphology and position clearly identified this strong but previously unidentified radio source with a bright 13-magnitude star with a wisp (jet) of optical emission. Schmidt (1963) obtained an optical spectrum of the star and interpreted the lines as having a redshift of 0.15.

Parkes is operated by CSIRO as a national facility with open sky access policy.

12.6 Arecibo

In 1963 at Arecibo, Puerto Rico, the US constructed the largest single aperture reflecting dish ever built. This has a 1,000-ft diameter but is a fixed spherical reflector with a movable focus. Originally designed for prime focus with a line feed, it was modified to a Gregorian with a 22-m correcting sub-reflector (Goldsmith 1996). A major component of the Arecibo telescope is the powerful radar system which enables the observatory to make radar observations of asteroids, comets, planets, and planetary satellites.

The Arecibo 1,000-ft dish was designed by Bill Gordon in the 1950s for ionospheric backscatter experiments, not for radio astronomy. It later became apparent that Gordon had overestimated the spectral width of the returned echoes in calculating the dish size needed to detect echoes from the ionosphere, and that a much smaller (and very much cheaper) dish

would be sufficient for the ionosphere experiments. However, by then, enthusiasm for a 1,000-ft dish had grown, and Gordon was able to obtain construction funds from the military who were obsessed with anything that they might learn about the ionosphere in order to detect incoming Russian missiles (Cohen, 2008, private communication), and the Arecibo telescope was built as designed (Kellermann et al. 2009).

Arecibo was operated by Cornell University since it commenced operation until 2011 when the NSF operational contract was moved to a consortium including SRI international, USRA, and University of Puerto Rico. Arecibo is a national facility, funded by the NSF with open sky access policy.

12.7 Effelsberg 100-m Telescope

The Max Planck Institute, 100-m dish in Effelsberg near Bonn, is a classical steerable parabolic dish completed in 1972. It is one of the largest fully steerable dishes in the world.

The antenna has a primary mirror 100 m in diameter and a 6.5-m secondary mirror. It operates at frequencies between 0.300 and 96 GHz. Receivers are mounted at both the primary focus and at the secondary focus of the telescope enabling rapid changes between some receivers.

The high sensitivity and good performance of the 100 m made it an excellent tool for studying the 22-GHz water vapor line both as a single dish and as the highest S/N element in VLBI observations. The first extragalactic water vapor line was found by Churchwell et al. (1977).

This very well known 408-MHz all-sky image (*Fig. 8-8*) is from the Effelsberg 100-m telescope and the Parkes telescope (for the Southern Hemisphere). It was produced by Haslam et al. (1982) and is now the basis for the estimation of foreground nonthermal contributions to the CMB radio emission.

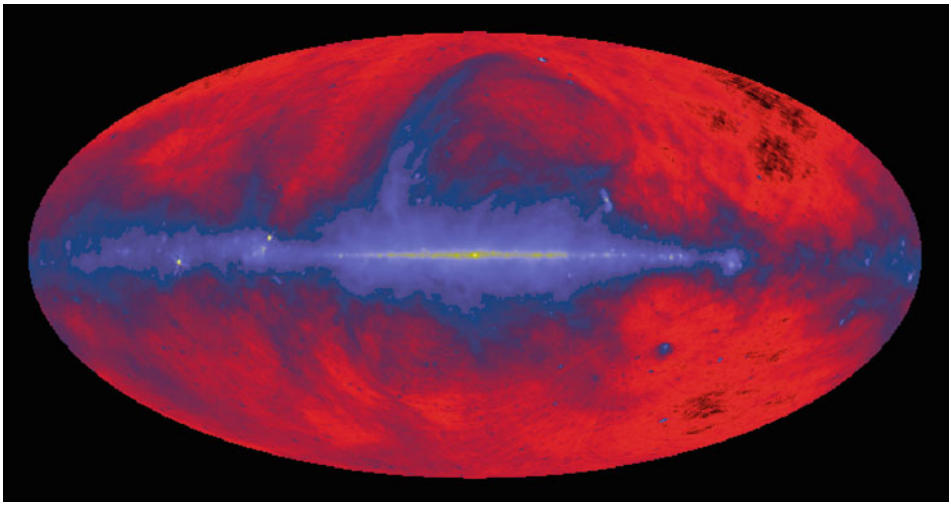

Fig. 8-8
All-sky radio emission at 408 MHz (Haslam et al. 1982)

The 100-m Effelsberg radio telescope of the Max-Planck-Institut für Radioastronomie is made available to all qualified scientists. The present policy allows the allocation of up to 40% of available observing time to visitors.

12.8 Green Bank Telescope (GBT)

The Robert C. Byrd 100-m Green Bank Telescope (GBT), replacing an older transit dish, is the last of the giant dishes to be built. It commenced operation in 2000. Unlike its predecessors, the GBT is an off-axis segment of a parabola with offset focus (both prime and Gregorian) which provides an unblocked aperture for high efficiency and minimum spectral ripple. It is one of the largest fully steerable dishes in the world.

At the same Green Bank observatory, you will now also find the original Grote Reber dish which was reassembled there by Reber in 1960, and a reconstruction of Jansky's telescope.

The GBT is operated by NRAO as a National Science Foundation facility with open sky access policy.

12.9 Westerbork Synthesis Radio Telescope (WSRT)

The forerunner of the Westerbork telescope was the Benelux Cross,[1] a joint Netherlands-Belgium project initiated by Professor Jan Oort in 1958 to use the radio astronomy source counts for cosmology.

The design was drastically modified under the influence of Jan Hogbom, a recent Ph.D. graduate from Ryle's group in Cambridge, and Chris Christiansen, from CSIRO in Sydney. The Benelux Cross was transformed into the Westerbork Synthesis Radio Telescope (WSRT) which combined aspects of aperture synthesis using movable elements and Earth rotation synthesis, from Cambridge, with the grating array concepts, from Australia. The WSRT opened in 1970 (Hogbom and Brouw 1974). In 1980, it was extended from twelve to fourteen 25-m dishes and from 1.5- to 3-km maximum E–W baseline. With its much greater sensitivity, the WSRT was able to make great advances in HI synthesis imaging and to open up areas of galactic astronomy with the observations of HII regions, interacting binaries and the Galactic Center. A phased array feed (PAF) system, called APERTIF, is being installed in the WSRT. APERTIF will cover frequencies from 1.0 to 1.7 GHz, increasing the instantaneous FoV of the WSRT to 8 deg^2 (Oosterloo et al. 2010).

Westerbork is operated by ASTRON, Netherlands Institute for Radio Astronomy, as an open access user facility.

12.10 Jodrell Bank

For over 50 years, the giant Lovell telescope at Jodrell Bank has been an internationally renowned landmark in the world of astronomy. It has been operating since the summer of 1957,

[1] http://www.astron.nl/radio-observatory/public/history-wsrt/benelux-cross-antenna-project/benelux-cross-antenna-project.

just in time for the launch of Sputnik. It is a fully steerable 76-m (250-ft) parabolic antenna with receivers at the prime focus.

The Jodrell Bank 250-ft radio telescope was originally designed to detect radio echoes from cosmic ray air showers. Although this was not possible because the fast recombination in the ionized cosmic ray trail suppresses the echo below detectability, the 250-ft parabolic reflector was built in the 1950s with an upgraded surface so it could reach the 21-cm hydrogen line which was discovered in 1951. The latest upgrade took place in 2002 giving good performance at frequencies above 5 GHz.

The Lovell telescope, used as an interferometer with small telescopes, found that some radio sources had exceedingly small angular size. These were eventually identified with high-redshift stellar counterparts – the quasars.

Jodrell Bank is operated by the University of Manchester.

12.11 Giant Meterwave Radio Telescope (GMRT)

The GMRT was built near Pune in India in 1995. It is an array of 30 large fully steerable 45-m dishes and occupies a key niche for very high sensitivity at intermediate and lower radio frequencies (50 MHz–1.5 GHz). It is a 2D array with a range of baselines up to 20 km, giving an angular resolution of $1''$ at 21 cm. Although it was not in the top list of telescopes in Trimble and Ceja (2010), its impact has increased rapidly since then.

GMRT is operated by the National Center for Radio Astrophysics, a part of the Tata Institute of Fundamental Research, with open sky access policy.

13 Future Big Science Projects in Radio Astronomy

13.1 The Karl G Jansky Very Large Array (JVLA, Previously the EVLA)

After 30 years with only minimal upgrades, the VLA is undergoing a major upgrade, and the Expanded VLA is now coming into operation with 5–20 times the sensitivity, almost complete frequency coverage, and greatly enhanced spectral capability. This illustrates the dramatic impact of improved technology even though the collecting area has not changed (Perley et al. 2011).

The Expanded VLA will be known as the Karl G Jansky Very large Array (JVLA).

13.2 ALMA

This major new mm and sub-mm array is covered in Chap. 7, "Submillimeter Telescopes."

13.3 LOFAR

LOFAR is a €150-million Dutch-led project building a novel low-frequency-phased aperture arrays spread over northern Europe. It is an all-electronic telescope covering low frequencies

from 30 to 80 MHz and 120–240 MHz. The array still has some sensitivity below 30 Mhz, and it may be possible to do some astronomical observations in this range. In Europe, FM radio occupancy of the band between 80 and 120 MHz makes this band unusable for radio astronomy. LOFAR will begin its operational phase in mid 2012 following a period of commissioning in 2010 and 2011.

13.4 Murchison Widefield Array (MWA)

Construction of the MWA began in February 2012. It is an all-electronic-phased array with no moving parts, observing at frequencies from 80 to 300 MHz, and located in the radio-quiet Western Australia Outback. The majority of the array tiles are concentrated into a 1.5-km core.

The MWA is an international collaboration between institutions from the US, Australia, New Zealand, and India.

13.5 Long Wavelength Array (LWA)

A phased array with plans for 53 stations each comprising 256 dipoles operating in the radio frequency range of about 20–80 MHz. The core is located at the VLA site, and baselines will eventually extend to 400 km.

The Long Wavelength Array project is a consortium led by the University of New Mexico, and includes the Los Alamos National Laboratory, the United States Naval Research Laboratories, and NASA's Jet Propulsion Laboratory.

13.6 FAST

FAST was originally conceived as an element of a future SKA proposal with a small number of large elements. It is now being developed as a single very large 500-m Arecibo-like dish. It is being built in the karst region of Guizhou province in China and uses an innovative stretched membrane structure to deform the spherical dish into a parabolic shape rather than using a line feed or a large correcting secondary mirror. It is now under construction and is expected to be completed by 2016.

13.7 SKA and the SKA Precursors

The SKA precursor facilities are being developed to demonstrate technology needed for the SKA. The two SKA precursor facilities under construction are MeerKAT and ASKAP.

13.7.1 MeerKAT

MeerKAT is a South African project to build an array of sixty-four 13.5-m diameter dishes located near Carnarvon in the Northern Cape province of South Africa. MeerKAT is part of the technology development required for the SKA. The full MeerKAT array is expected to be

ready by 2015–2016. The dishes will be equipped with a number of high-performance single pixel feeds to cover frequencies from 580 MHz up to 14 GHz.

13.7.2 ASKAP

The Australian SKA Pathfinder, ASKAP, is a project to build a telescope array of thirty-six 12-m dishes. It will be testing advanced, innovative technologies such as phased array feeds and a three axis mount to give a wide field of view (30 deg^2) with very high dynamic range (DeBoer et al. 2009).

ASKAP is being built by CSIRO at the Murchison Radio-astronomy Observatory site, an extremely low RFI environment, located near Boolardy in the Midwest region of Western Australia. All 36 antennas and their technical systems are expected to be completed in 2014.

13.7.3 SKA

The Square Kilometer Array (SKA) is a proposed radio telescope with a total collecting area of approximately one square kilometer, a frequency range from 70 MHz to 25 GHz and baselines up to at least 3,000 km from a concentrated central core. The SKA will be built in the southern hemisphere, in either South Africa or Australia. Construction of the SKA is scheduled to begin in 2016 for initial observations by 2019 and full operation by 2024.

The design will use aperture array technology for the lower frequencies and arrays of parabolic dishes at the higher frequencies. To provide a square kilometer of aperture at an acceptable cost, the SKA must make a revolutionary break with current radio telescope design. Some aspects of the technology needed are still in the development stage, and the various SKA precursors are now exploring some of the key technologies.

The construction will be a major undertaking and will be implemented in phases. Phase 1 is the initial deployment (15–20%) of the array at mid-band frequencies, Phase 2 is the full collecting area at low- and mid-band frequencies (~70 MHz–10 GHz), and Phase 3 sees the implementation at higher frequencies of 25 GHz or more.

The key science areas driving the current SKA are described in detail in "Science with the Square Kilometer Array" (Carilli and Rawlings 2004).

14 The Future

As discussed in Sect. 2.2.2 , the growth of radio astronomy facilities has been exponential since the beginning in 1940, but how do we maintain exponential growth? If the improvement in sensitivity has reached a ceiling, the rates of new discoveries will decline and the field will become uninteresting and slowly die. On the other hand, if we can shift to new technology or find new ways to organize our resources, the exponential increase in sensitivity can continue. Do we have such new technology to continue the exponential improvement? In radio astronomy, the combination of transistor amplifiers and their large scale integration into complex systems which can be duplicated inexpensively provides one of the keys for change. The other key technology is the computing capacity to apply digital processing at high bandwidth

thereby realizing processes such as multiple adaptive beam formation and active interference rejection in ways not previously conceivable. Finally, the move to international facilities such as the proposed SKA will also be needed to avoid the resource ceiling.

Appendix

A.1. Optical and Radio Analogs and Terminology

Radio	Optical
Antenna, dish	Telescope, element
Sidelobes	Diffraction pattern
Near sidelobes	Airy rings
Feed legs	Spider
Aperture blockage	Vignetting
Dirty beam	Point spread function (PSF)
Primary beam	Field of view
Map	Image
Source	Object
Image plane	Image plane
Aperture plane	Pupil plane
UV plane	Fourier plane
Aperture	Entrance pupil
UV coverage	Modulation transfer function
Grating responses	Aliased orders
Primary beam direction	Grating blaze angle
UV (visibility) plane	Hologram
Bandwidth smearing	Chromatic aberration
Local oscillator	Reference beam
Dynamic range	Contrast
Phased array	Beam combiner
Correlator	*No analog*
No analog	Correlator
Receiver	Detector
Taper	Apodise
Self-calibration	Wavefront sensing (adaptive optics)

A.2. The World's Largest Centimeter and Meter Radio Telescopes

Notes on the Table A.2:

Only operating radio telescopes with diameter greater than 25 m (or equivalent area) are included. Note that this excludes many of the important smaller mm telescopes. For simplicity, the geometric areas are given. Effective areas (see Sect. 4.2.1) will be less and depend on

Country	Name	Latitude	Longitude (east)	Frequency range (GHz)		No	Size (m)	Area (sqm)	Type
Argentina	IAR	−34.88	−58.14	1.42	1.72	2	30	1,414	Dish
Australia	ATCA – Narrabri	−30.31	149.55	1.30	106	6	22	2,281	Dish array
Australia	Ceduna	−31.87	133.81	2.20	22	1	30	707	Dish
Australia	DSS43 Tidbinbilla	−35.41	148.98	1.70	22	1	70	3,848	Dish
Australia	Hobart	−42.81	147.44	1.40	22	1	26	531	Dish
Australia	MOST	−35.37	149.42	0.84	0.84	2	778 × 12	9,336	Cylinder cross
Australia	Parkes	−33.00	148.26	0.44	24	1	64	3,217	Dish
Canada	DRAO – synthesis telescope	49.32	−119.62	0.41	1.42	7	8.5	397	Dish array
Canada	DRAO 26-m	49.32	−119.62	1.42	1.67	1	26	531	Dish
China	Shanghai	31.10	121.20	1.62	22.6	1	25	491	Dish
China	Urumqi	43.50	87.18	0.31	24	1	25	491	Dish
France	IRAM – Plateau de Bure	44.63	5.91	0.08	230	3	15	530	Dish array
France	Nancay decametric array	47.38	2.20	0.01	0.08	144	2 × 3,500	3,526	Array
France	Nancay radio heliograph	47.38	2.20	0.15	0.45	44	5	864	Dish cross
France	Nancay radio telescope	47.38	2.20	1.30	3.3	1	200 × 40	8,000	Kraus type
Germany	Effelsberg	50.52	6.88	0.41	100	1	100	7,854	Dish
India	Gauribidanur	13.60	77.45	0.03	0.15	1	1,500 × 25	37,500	Array T
India	GMRT	19.10	74.05	0.38	1.67	30	45	47,713	Dish array
India	Ooty radio telescope	11.38	76.67	0.33	0.33	1	530 × 30	15,900	Cylinder
Italy	Medicina	44.52	11.65	0.32	3.5	1	32	804	Dish
Italy	Medicina northern cross	44.52	11.65	0.41	0.41		600 × 34	30,000	Cylinder T
Italy	Noto	36.88	14.99	1.33	43.5	1	32	804	Dish
Italy	Sardinia	39.50	9.24	0.41	100	1	64	3,217	Dish
Japan	Kashima	35.95	140.65	1.50	43	1	34	908	Dish
Japan	Nobeyama	35.94	138.48	1.40	116	1	45	1,590	Dish
Japan	Usuda	36.13	138.37	1.40	43	1	64	3,217	Dish
Japan	VERA	24–39	124–142	2.20	87	4	20	1,257	VLBI dishes
Korea	KVN	33–37	126–129	2.00	115	3	20	942	VLBI dishes
Mauritius	MRT	−20.13	57.73	0.15	0.15	1	2,000 × 2	25,000	Array T
Netherlands	Dwingeloo	52.81	6.40			1	25	491	Dish

Country	Name	Latitude	Longitude (east)	Frequency range (GHz)		No	Size (m)	Area (sqm)	Type
Netherlands	Westerbork	52.92	6.60	0.32	8.65	14	25	6,872	Dish array
Poland	Torun	52.91	18.56	0.15	6.95	1	32	804	Dish
Puerto Rico	Arecibo	18.34	−66.75	0.33	8.5	1	305	73,062	Fixed spherical
Russia	Kalyazin	57.22	37.90	0.61	22.5	1	64	3,217	Dish
Russia	KVAZAR	44–61	30–102	1.40	22.39	3	32	2,413	VLBI dishes
Russia	Puschino BSA	54.82	37.67	0.11	0.11	1		25,000	Phased array
Russia	Puschino DKR-1000	54.82	37.67	0.04	0.12	1	2 × 1,000	16,000	Cylinder cross
Russia	RATAN 600	43.83	41.59	1.00	22	1	2 × 1,812	3,624	Parabolic section
South Africa	Hartebeesthoek	−25.89	27.68	1.60	22	1	26	531	Dish
Spain	DSS63 Madrid	40.43	−4.25	1.70	22	1	70	3,848	Dish
Spain	IRAM – Pico Veleta	37.07	−3.39	1.61	360	1	30	707	Dish
Sweden	Onsala	57.40	11.93	1.33	116	1	25	491	Dish
UK	Cambridge – Ryle	52.17	0.04	0.04	31.8	8	13	1,062	Dish array
UK	Jodrell Bank – Lovell	53.24	−2.31	0.15	24	1	76	4,536	Dish
UK	Jodrell Bank – MkII	53.24	−2.31	0.15	24	1	25 × 28	550	Dish
UK	Merlin – Cambridge 32 m	52.17	0.04	0.15	24	1	32	804	VLBI dishes
UK	Merlin	52–54	−2 to −3	0.15	24	4	25	1,963	VLBI dishes
Ukraine	Evpatoriya	48.38	31.16	1.60	22	1	70	3,848	Dish
Ukraine	URAN 1-4	42–50	25–43	0.01	0.04	4			Interferometer
Ukraine	UTR-2 Grakovo	49.63	36.93	0.01	0.04	1	1,800 × 54 + 900 × 54	150,000	Array T
USA	DSS13 Goldstone	35.25	−116.79	2.30	8.4	1	26	531	Dish
USA	DSS14 Goldstone	35.43	−116.89	1.70	22	1	70	3,848	Dish
USA	Greenbank, 140′	38.44	−79.83	0.05	25.2	1	43	1,452	Dish
USA	Greenbank, interferometer	38.44	−79.83	2.10	8.6	2	26	1,062	Interferometer
USA	Haystack observatory	42.62	−71.49	2.20	115	1	36	1,018	Dish
USA	Owens Valley 40 m	37.00	−118.00	0.32	43.4	1	40	1,257	Dish
USA	Owens Valley interferometer	37.23	−118.29	0.50	18	2	27	1,145	Interferometer
USA	JVLA	34.08	−107.62	0.05	50	27	25	13,254	Dish array
USA	VLBA	17–48	−64 to −155	0.31	43.5	10	25	4,909	VLBI dishes

actual aperture efficiency which is a function of frequency. At best, both these will usually be 65% of the geometric area and sometimes much less. Upper and lower frequencies are based on available receivers rather than the antenna frequency range.

Groups of antennas used primarily as part of a VLBI array are not listed separately (e.g., VLBA antennas), and the range of coordinates given and number of antennas indicate the full extent of the array.

Longitude is given as an angular measurement ranging from 0° at the prime meridian to +180° eastward and −180° westward. For calculations, the west/east suffix is replaced by a negative sign in the western hemisphere. Confusingly, the convention of negative for east is also sometimes seen. We use the preferred convention that east be positive. Latitude south is minus.

References to Table A.2:

The most complete listings of radio telescopes and their operating frequencies are maintained by the three ITU radio astronomy spectrum management authorities:

CORF (North America) http://sites.nationalacademies.org/BPA/BPA_059065#list

CRAF (Europe) http://www.craf.eu/raobs.htm

RAFCAP (Asian Pacific) http://www.atnf.csiro.au/rafcap/AP_RT.htm

References

Akgiray, A., Weinreb, S., & Imbriale, W. A. 2011, Design and measurements of a dual-polarized wideband constant-beamwidth quadruple-ridged flared horn, in IEEE Antennas and Propagation International Symposium, Spokane, Washington DC, July 2011

Athreya, R. 2009, ApJ, 696, 885–890

Baars, J. W. M. 2007, The parabolic reflector antenna in radio astronomy and communications, in Astrophysics Science library (Heidelberg: Springer)

Barnbaum, C., & Bradley, R. F. 1998, AJ, 116, 2598–2614

Born, M., & Wolf, E. 1965, Principles of Optics (Oxford: Pergamon)

Bracewell, R. N. 1986, The Fourier Transform and Its Applications (2nd ed.; New York: McGraw Hill)

Brentjens, M. A., & de Bruyn, A. G. 2005, A&A, 441, 1217

Briggs, F. H., Bell, J. F., & Kesteven, M. J. 2000, AJ, 120, 3351–3361

Bunton, J. D. 2011, IEEE Trans. Antenna Propag., 59, 2041–2046

Burke, B. F., & Graham-Smith, F. 1996, An Introduction to Radio Astronomy (Cambridge, UK: Cambridge University Press)

Carilli, C. L., & Rawlings, S. 2004, New Astron. Rev., 48, 979–984

Christiansen, W., & Warburton, J. 1955, Aust. J. Phys., 8, 474–486

Christiansen, W. N., & Hogbom, J. A. 1985, Radiotelescopes (2nd ed.; Cambridge, UK: Cambridge University Press)

Churchwell, E. B., Witzel, A., Huchtmeier, W., Pauliny-Toth, I., Roland, J. & Sieber, W. 1977, A&A, 54, 969

Cooley, J. W., & Tukey, J. W. 1965, Math. Comput. 19, 297–301

Cordes, J. 2007 revised 2009, Survey Metrics. SKA Memo 109, http://www.skatelescope.org/publications/

Cornwell, T. J. 1988, A&A, 202, 316

Cornwell, T. J., Holdaway, M. A., & Uson, J. M. 1993, A&A, 271, 697

DeBoer, D. R., Gough, R. G., Bunton, J. D., Cornwell, T. J., Beresford, R. J., Johnston, S. Feain, I. J., Schinckel, A. E., Jackson, C. A., Kesteven, M. J., Chippendale, A., Hampson, G. A., O'Sullivan, J. D., Hay, S. G., Jacka, C. E., Sweeloam, T. W., Storey, M. C., Ball, L., & Boyle, B. J. 2009, Proc. IEEE, 97, 1507–1521

de Solla Price, D. J. 1963, Little Science, Big Science (New York, NY: Columbia University Press)

Ekers, R. D., & Bell, J. F. 2002, Radio frequency interference, in IAU Symposium 199: The Universe at Low Radio Frequencies, Pune, India, 30 November–4 December 1999, ed. A. Pramesh Rao, G. Swarup, & Gopal-Krishna, 498–505

Ekers, R. D., & Rots, A. H. 1979, in Image Formation from Coherence Functions in Astronomy, Proc. IAU Colloq. 49, Groningen, Netherlands, August 10–12, 1978, Astrophysics and Space Science Library. Vol. 76, ed. C. van Schooneveld (Dordrecht/Boston: Reidel), 61

Ellingson, S. W. 2005, Introduction to special section on mitigation of radio frequency interference in radio astronomy. Radio Sci., 40, RS5S01

Ellingson, S. W., Bunton, J. D., & Bell, J. F. 2001, ApJSS, 135, 87–93

Fisher, J. R., & Bradley, R. F. 2000, Proc. SPIE, 4015, 308–318. Radio Telescopes, ed H. R. Butcher

Frater, R. H., Brooks, J. W., & Whiteoak, J. B. 1992, J. Electr. Electron. Eng. Aust., 12, 103–12

Goldsmith, P. F. ed. 1988, in Instrumentation and Techniques for Radio Astronomy (New York: IEEE)

Goldsmith, P. F. 1994, Quasioptical Systems: Gaussian Beam Quasioptical Propagation and Applications (New York: Wiley/IEEE)

Goldsmith, P. F. 1996, IEEE, 15, 38–43

Goris, M. 1998, Categories of Radio Interference, NFRA Technical Report – 415/MG/V2.3

Harwit, M. 1981, Cosmic Discovery – The Search, Scope and Heritage of Astronomy (New York, NY: Basic Books)

Haslam, C. G. T., Salter, C. J., Stoffel, H., & Wilson, W. E. 1982, A&A Suppl 47, 1

Hay, S., O'Sullivan, J., & Mittra, R. 2008, IEEE Antennas and Propagation Society International Symposium, AP-S, San Diego, CA, July 5–11 2008, 1–4

Hazard, C., Mackey, M. B., & Shimmins, A. J. 1963, Nature, 197, 1037–1039

Herrnstein, J. R., Moran, J. M., Greenhill, L. J., Diamond, P. J., Inoue, M., Nakai, N., Miyoshi, M., Henkel, C., & Riess, A. 1999, Nature, 400, 539–541

Hogbom, J. A., & Brouw, W. N. 1974, A&A, 33, 289

Jansky, K. G. 1933a, Nature, 132, 66

Jansky, K. G. 1933b, Proc. IRE, 21, 1387–1398

Jenkins, F. A., & White, H. E. 2001, in Fundamentals of Optics (4th ed.; New York: McGraw-Hill)

Kawaguchi, N., Sasao, T., & Manabe, S. 2000, in Radio Telescopes, ed H. Butcher, Proc. SPIE, Vol. 4015 (Washington, DC: SPIE), 544–551

Kellermann, K. I., Cordes, J. M., Ekers, R. D., Lazio, J., & Wilkinson, P. N. 2009, in Accelerating the Rate of Astronomical Discovery – SPS5, IAU GA, Rio de Janeiro, Brazil, August 11–14

Kellermann, K. I., & Moran, J. M. 2001, Ann. Rev. A&A, 39, 457–509

Kesteven, M. 2010, Proc. RFI Mitig. Workshop, 29–31 March 2010. Groningen, the Netherlands. PoS(RFI2010)007

Kildal, P.-S., Jian Yang, Karandikar, Y., Wadefalk, N., Pantaleev, M., & Helldner, L. 2009, Development of a coolable 2–14 GHz Eleven feed for future radio telescopes for SKA and VLBI 2010, in Electromagnetics in Advanced Applications, 2009. ICEAA '09, Turin, Italy, 545–547

Kraus, J. D. 1986, Radio Astronomy (2nd ed.; Powell, OH: Cygnus-Quasar)

Large, M. I., Campbell-Wilson, D., Cram, L. E., Davison, R. G., & Robertson, J. G. 1994, Astron. Soc. Aust. Proc. 11, 44–49

Livingston, M. S., & Blewett, P. 1962, Particle Accelerators (New York: McGraw Hill)

Love, A. W. ed. 1976, in Electromagnetic Horn Antennas (New York: IEEE)

Machin, K. E. 1951, Nature, 167, 889–89

Macquart, J.-P., Ekers, R. D., Feain, I., & Johnston-Hollitt, M. 2012, ApJ, 750, 15

McCready, L. L., Pawsey, J. L., & Payne-Scott, R. 1947, Proc. R. Soc. A, 190, 357–375

Mills, B. Y., & Little, A. G. 1953, Aust. J. Phys., 6, 272

Miyoshi, M., Moran, J., Herrnstein, J., Greenhill, L., Nakai, N., Diamond, P., & Inoue, M. 1995, Nature, 373, 127–129

Mollick E. 2006, Establishing Moore's law. IEEE Ann. History Comput., 28(3), 62–75

Moore G. E. 1965, Cramming more components onto integrated circuit. Electronics, 38, 8

Nagel, J. R., Warnick, K. F., Jeffs, B. D., Fisher, J. R. & Bradley, R. 2007, Radio Sci., 42, RS6013

Napier, P. J., Thompson, A. R., & Ekers, R. D. 1983, Proc. IEEE, 71, 1295–1320

O'Brien, P. A. 1953, MNRAS, 113, 597–612

Oosterloo, T., Verheijen, M., & van Cappellen, W. 2010, in Proc. ISKAF2010 Sci. Meet., June 10–14 2010, Assen, the Netherlands, PoS(ISKAF2010) 043

Perley, R. A., Chandler, C. J., Butler, B. J., & Wrobel, J. M. 2011, ApJL, 739, L1

Radhakrishan, V., 1990, in Modern Radio Science, from URSI General Assembly, Prague, Czechoslavakia, ed J. Bach Anderson (Published for the International Union of radio Science and the ICSU Press by Oxford University Press, UK), 187

Radhakrishnan, V. 1999, in Synthesis Imaging in Radio Astronomy II, A Collection of Lectures from the Sixth NRAO/NMIMT Synthesis Imaging Summer School, ASP Conf. Ser. 180, ed. G. B. Taylor, C. L. Carilli, & R. A. Perley (San Francisco, CA: ASP), 671

Reber, G. 1958, Proc. IRE, 46, 15–23

Reed, J. H. 2002, Software Radio: A Modern Approach to Radio Engineering (Upper Saddle River, NJ: Prentice Hall)
Reich, W., Kalberla, P., Reif, K., & Neidhöfer, J. 1978, A&A, 76, 92
Riesselmann, K. 2009, Deconstruction: Livingston plot. Symmetry, 6, 30
Ryle, M. 1952, Proc. R. Soc. Lond. A, 211(1106), 351–375
Ryle, M., & Hewish, A. 1960, MNRAS, 120, 220
Ryle, M., & Neville, A. C. 1962, MNRAS, 125, 39
Ryle, M., & Vonberg, D. D. 1946, Nature, 158, 339–340
Schmidt, M. 1963, Nature, 197, 1040–1041
Stanier, H. M. 1950, Nature, 165, 354–355
Sullivan, W. T. 2009, Cosmic Noise (New York, NY: Cambridge University Press)
Taylor, G. B., Carilli, C. L., & Perley, R. A. 1999, Synthesis Imaging in Radio Astronomy II, A Collection of Lectures from the Sixth NRAO/NMIMT Synthesis Imaging Summer School. ASP Conf. Ser. 180 (San Francisco, CA: ASP)
Tegmark, M., & Zaldarriaga, M. 2010, Phys. Rev. D, 82, id. 103501
Thompson, A. R., Moran, J. M., & Swenson, G. W. 2001, Interferometry and Synthesis in Radio Astronomy (New York, NY: Wiley)
Trimble, V., & Ceja, J. A. 2010, Astron. Nachr., 331, 338
Wild, J. P. 1967, Proc. Instn. Radio Electron. Engrs. Aust., 28(9), 279–291
Wilkinson, P. N., Kellermann, K. I., Ekers, R. D., Cordes, J. M., & Lazio, T. J. W. 2004, The exploration of the unknown. New Astron. Rev., 48(11–12), 1551–1563
Wilson, T. L., Rohlfs, K., & Hüttemeister, S. 2008, Tools of Radio Astronomy (5th edn.; Heidelberg: Springer)
Wilson, W. E., Ferris, R. H., Axtens, P., Brown, A., Davis, E., Hampson, G., Leach, M., Roberts, P., Saunders, S., Koribalski, B. S., et al., 2011, MNRAS, 416, 832–56
Zanardo, G., Staveley-Smith, L., Ball, L., Gaensler, B. M., Kesteven, M. J., Manchester, R. N., Ng, C.-Y., Tzioumis, A. K., & Potter, T. M. 2010, ApJ, 710, 1515–1529